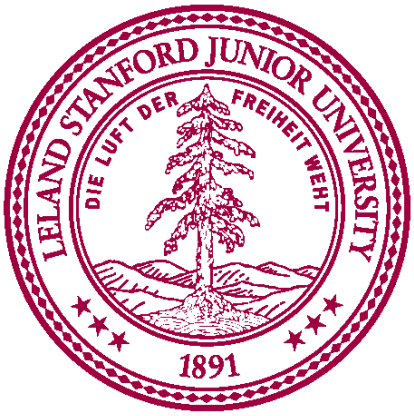

Albert-Ludwigs-University of Freiburg
Bachelor of Science in Biology
Bachelor thesis

Quantitative in silico and in vivo characterization of the recombinase addressable data storage

Nicolas Koutsoubelis

Written at the Stanford University, USA
Department of Bioengineering
Laboratory Prof. PhD. Drew Endy

Submitted: 16. July 2012
Supervisor Freiburg: Prof. PhD. Wilfried Weber
Supervisors Stanford: Prof. PhD. Drew Endy, PhD (can) Pakpoom Subsoontorn

Acknowledgements

“The walls are there for a reason. The walls are not there to keep us out; the walls are there to give us a chance to show how badly we want something.” (Randy Pausch)

At first I want to thank Prof. Drew Endy. I thank him for the courage of taking a foreign student, for the confidence that he has placed in me and for giving me the opportunity to make this wonderful experience. People with this kind of courage are needed!
I also want to thank Prof. Weber that with his supervision it was possible for me to take this adventure.
Especially I want to thank my supervisor Pakpoom Ton Subsoontorn, for the uncountable hours of explaining and correcting. Also I thank him for the happiness and motivation for our project. He was a great supervisor and I hope to be a good fried for him in the future. As well as I thank Ton, I want to thank Jerome Bonnet for the many different kinds of support, the corrections, for the tricks in the wet lab work and the cheering up! Also I want to thank Monica and Paul for their support and good talks.
At least my thank goes to all the people that stand behind me! The people that sing the melodies of my heart for me when I did not hear it, named as my lovely mum Annemarie Krink and my wonderful friend Anne Löchner.

Table of contents

Abbreviations

Amp	Ampicillin
ampR	Ampicillin resistance cassette
ara	Arabinose
aTc	Anhydrotetracycline
Bb	Backbone plasmid
Cam	Chloramphenicol
camR	Chloramphenicol resistance cassette
CPEC	Circular Polymerase Extension Cloning
FACS	Fluorescent activating cell sorting
int	Integrase
KAN	Kanamycine
kanR	Kanamycine resistance cassette
LB media	Lysogene broth media
orf	Open reading frame
ori	Origin of replication
PCR	Polymerase chain reaction
RAD module	Recombinase addressable data storage module
rRAD model	Realistic reaction rate RAD model
RBS	Ribosomal binding site
xis	Excisionase

Abstract

Synthetic biological memory devices have many applications in biotechnology as well as in basic research, for example as a study tool for aging research.
In the recently published work, Bonnet, Subsoontorn et al. engineered a recombinase addressable data (RAD) storage module that can store 1bit of information in living cells by using serine integrase and excisionase to invert and revert a piece of DNA. This DNA piece functions as data register. The switch of the DNA data register between one of two states is a result of a distinguished input that activates the integrase or excisionase. The RAD module offers several advantages over other engineered genetically encoded memory devices, including the ability of rewriting states and of storing states in the absence of heterologous gene expression.
Although the published work (Bonnet, Subsoontorn et al. 2012) already presents an example of a robustly functional RAD module, the quantitative understanding of the RAD module operation is limited. In particular, an input-output function of the RAD module has not been experimentally characterized and an existing mathematical model of RAD operations is not based on realistic physical parameters.
The following bachelor thesis aimed exploring the input-output relationship of the RAD module. The work was divided into a computational and an experimental part.
For the computational part we generated an improved version of the model published in the Bonnet, Subsoontorn et al. paper that includes more realistic reaction rates and can easily be improved by adding data from experimental measurements. In parallel, we built a teaching model that in future can be used to teach students computational modeling of DNA recombination.
For the experimental part we built and characterized the RAD module in a new bacterial chassis that allows linear induction of the promoters controlling the RAD module, and successfully measured the level of promoter activity that is required to drive a recombination event for both writing and rewriting operations. By transferring the RAD module into this new genetic background, we also observed some significant changes in its behavior, emphasizing the need of a careful optimization of the device in its particular context of operation.
This work, along with the tools and methodologies that we developed, represents a first step towards a precise quantitative understanding of the operational constraints of the RAD module and will support future composition of RAD modules into higher order devices for various applications.

Zusammenfassung

Synthetisch biologische Speicherbauteile haben viele Anwendungsmöglichkeiten im Bereich der Biotechnologie. Auch in der Grundlagenforschung können sie zum Beispiel als Werkzeuge für die Altersforschung dienen. In der kürzlich veröffentlichten Arbeit entwickelten Bonnet, Subsoontorn et al. ein auf einer Rekombinase beruhendes adressierbares Speichermodul (RAD), welches 1bit an Information in lebenden Zellen speichern kann. Das System nutzt eine Serin-Integrase und -Excisionase, um ein DNA Stück auszuschneiden und in umgekehrter Richtung wieder einzubauen. Dieses DNA Stück fungiert somit als Speichereinheit. Die Umkehr des DNA Stückes, der Speichereinheit, zwischen einem der beiden möglichen Zustände ist das Ergebnis eines bestimmten Inputs, welcher die Integrase oder die Excisionase aktiviert. Obwohl die publizierte Arbeit (Bonnet, Subsoontorn et al. 2012) schon ein Beispiel für ein robustes RAD Modul ist, ist unser quantitatives Verständnis für die Operabilität des RAD Moduls begrenzt. Insbesondere auf die Input-Output-Funktion bezogen ist das RAD Modul noch nicht ausreichend experimentell charakterisiert. Auch gab es bisher kein mathematisches Modell für das RAD, welches physikalisch realistische Parameter beinhaltet.
Die folgende Bachelorarbeit hatte nun das Ziel, die Input-Output Beziehung des RAD Moduls zu charakterisieren. Dafür wurde die Arbeit in einen computergestützten und einen experimentellen Teil untergliedert.
Im computergestützten Teil generierten wir eine verbesserte Version des bereits von Bonnet et al. veröffentlichten Modells, welches realistischere Reaktionsraten verwendet. Auch ist die verbesserte Version so entwickelt worden, dass es einfach ist, neues Wissen, welches durch experimentelle Messungen erhalten werden kann, in das Modell zu integrieren. Gleichzeitig haben

wir ein Lehrmodell entwickelt, welches in Zukunft dazu genutzt werden kann, Studenten computergestütztes Erstellen von Modellen von DNA Rekombinase Systemen näher zu bringen.
Für den experimentellen Teil haben wir das RAD Modul in ein neues Chassis eingebracht, das uns die Charakterisierung über eine lineare Induktion der RAD kontrollierenden Promotoren erlaubt. Wir haben erfolgreich das Level der Promotoraktivität gemessen, welches nötig ist, um ein Rekombinationsereignis für das „Schreiben und Überschreiben“ zu erreichen. Durch den Transfer des RAD Moduls in eine genetisch neue Umgebung haben wir außerdem einige beachtliche Veränderungen im Verhalten des RAD Moduls beobachtet, welche die Wichtigkeit einer vorsichtigen Optimierung des Moduls in diesem besonderen Zusammenhang hervorheben.
Die folgende Arbeit stellt mit den von uns entwickelten Werkzeugen und Methoden einen ersten Schritt zum quantitativen Verständnis des RAD Moduls dar. Diese Arbeit wird zukünftige Studien unterstützen können, wenn das RAD Modul in komplexere Systeme für verschiedenste Anwendungen übertragen werden soll.

1 Introduction

Synthetic Biology aims the rational engineering of biological systems for various applications. Synthetic biology transfers the ideas of engineering to biology. The engineering cycle typically includes five steps: defining the engineering aim, system design, computational study, construction of the system and system validation.
This engineering cycle can be repeated multiple times, until the product exceeds the initial requirements. The use of the engineering cycle allows synthetic biologists to rationally engineer living cells with novel capabilities that do not exist in nature. Notable achievements, including the synthesis of artemisinic acid (Ro, Paradise et al. 2006) by microorganisms, a potent antimalarial drug, various kinds of biomolecular computation or the engineering of cells that can perform behavior like logic gates, have been reached within the last years.
Among the diverse functions (sensors, processors, actuators) required for synthetic biological systems, biological memory devices can be beneficial to myriad of applications (Ham, Lee et al. 2008; Burrill and Silver 2010; Bonnet, Subsoontorn et al. 2012). Memory is a fundamental part of sophisticated behavior. It enables the tracking of particular events in time, as well as the implementation of sequential logic. In basic research, memory can be used as a study tool to gather information about the history of cells (Fig. 1), such as the number of cell divisions. Biological memory devices can also be used to program industrial microbes to respond to history of environmental conditions in a growth chamber.
In medicine, biological memory devices can be used to program "microbial robots" to release therapeutic molecules in response to specific sequences of the patient physiological states.

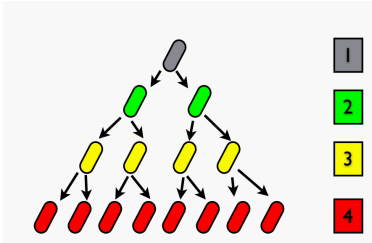

Fig. 1 Schematic for recording and reporting cell history – memory as a study tool for developmental biology. The cell counts the number of cell divisions. Generated by Pakpoom Subsoontorn.

Many different projects were published with different architectures and designs for biological memory devices (Tab. 1).

Tab. 1 Current data storage systems. Presenting storage mechanisms, activating input, rewritability, modularity and storage capacity. Generated by Pakpoom Subsoontorn, changed with his permission.

Reference	Mechanism	Input(s)	Re-writable	Modular	Capacity (bit)
Podhajska et al., 1985	DI	Heat shock inducing integrase expression	No	Yes	1
Toman et al., 1985	MI	DNA damaging agents inducing cI degradation	No	No	1
Gardner et al., 2000	MI	IPTG inactivating lacI; heat shock inactivating cIts; aTc inactivating tetR	Yes	No	1
Becskei et al., 2001	PAR	Doxycycline activating rtTA	No	No	1
Atkinson et al., 2003	PAR	IPTG inactivating lacI that represses NtrC production	Yes	No	1
Isaacs et al., 2003	PAR	Heat shock inactivating cIts	No	No	1
Kramer et al., 2004	MI	Pristinamycin I inactivating streptomycin; erythromycin inactivating macrolide	Yes	No	1
Kobayashi et al., 2004	MI	DNA damaging agents inducing cI degradation; IPTG to inactivating lacI; AHL inducing extra lacI production	Yes	Yes for set / No for reset	1
Maeda & Sano, 2006	PAR	IPTG inactivating lacI that represses cI production	Yes	No	1
Ham et al., 2006	DI	Arabinose inducing fimE expression	No	Yes	1
Ajo-Franklin et al., 2007	PAR	Galactose inducing extra VP64 activator production	No	Yes	1
Ham et al., 2008	DI	Arabinose and aTc independently inducing fimE and Hin expression	No	Yes	2
Friedland et al., 2009	DI	Arabionose inducing cre and flp expression cascade	No	Yes	2
Lou et al., 2010	MI	UV inducing cI and cI434 degradation	No	No	1
Moon et al., 2010	DI	Arabinose inducing fimE expression	No	Yes	1

DI = DNA inversion, MI = bistability of two mutually inhibiting genes, PAR = single positive auto-regulating genes

In the following chapter we will briefly summarize the state of the art in the engineering of synthetic biological memory devices.

There are basically two mechanisms to store information in biological systems: (i) bistable switch feedback loops and (ii) genetic memory systems, relying on direct DNA modification (mostly DNA inversion).

In an early work by Podhajska et al. a two state system based on phage lambda integrase was developed (Podhajska, Hasan et al. 1985). Through an induced impulse, integrase is expressed. That causes the inversion of the promoter and turns expression of a downstream gene on, i.e. switching the system from OFF to ON. After inversion, the presence of integrase is not required for maintaining and inheriting the ON state. The system is capable of storing 1bit of information, but it is not capable of reverting to the OFF state, if it has once reached the ON state. That means the system is not rewritable.

Gardner et al. (2000) proposed a system that uses bistable regulatory gene networks (Gardner, Cantor et al. 2000). The construct consists of two repressible promoters. Each promoter controls the gene expression of a repressor, which inhibits the other promoter. Two different inducers can regulate the inhibition of the repressors and can trigger state switching. With this system 1bit of information can be stored and the system is rewritable (Fig. 2). However, a constant protein synthesis is required to store the state, which makes the system sensitive for evolutionary counter-selection. A memory device based on bistability of mutually repressing genes, like the Gardener et al. system, has also been implemented in mammalian cells (Kramer, Viretta et al. 2004).

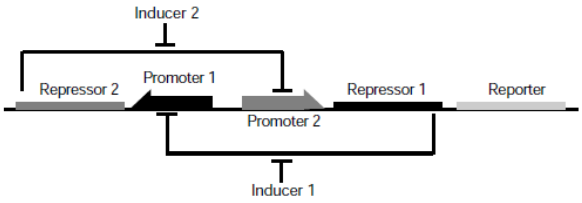

Fig. 2 Scheme of a genetic toggle switch. The first repressor (1) is induced by the first inducer (1) and inhibits the transcription of the first promoter (1). The second repressor (2) is induced by the second inducer (2) and inhibits the second promoter (2)(Gardner, Cantor et al. 2000).

Ham et al. engineered another system using DNA inversion. They designed a system with an artificial switch with overlapping inversions. A switch of this recombination site functions by the Fim integration system of *E.coli* and the Hin integration system of *Salmonella*. Their double inversion system is able to show four different states. Hence this system is able to store and inherit 2bit of information. Like the system by Podhajska et al., this system is not rewritable.

Despite each system having its own particular advantages, all of them fail in at least one of the three major needs: modularity, rewritability and heredity. Systems that use bistable, cross or auto regulations are likely unstable because of evolutionary counter-selection. The published systems that use DNA as data storage are only unidirectional and not rewritable. This is a problem in terms of scaling up the system to store more than 2bit of information. A scaling up to a useful 8bit memory is nearly impossible. However as soon as a memory device is rewritable, combinatorial architectures can be used to enable the exponential increase of storage capacity. An ability to exponentially scale up storage capacity is important because many important possible applications, such as lineage tracking in aging or developmental studies, require up to dozen or hundred states of storage. The recently published rewritable addressable data (RAD) storage (Fig. 3) is modular, rewritable and can be inherited. The device is able to store 1bit of information and can keep it over several generations. Because it uses DNA for data storage, counter-selection is no problem. Because of its rewritability, the RAD module will support combinatorial architectures to store multiple bits with a combinational code.

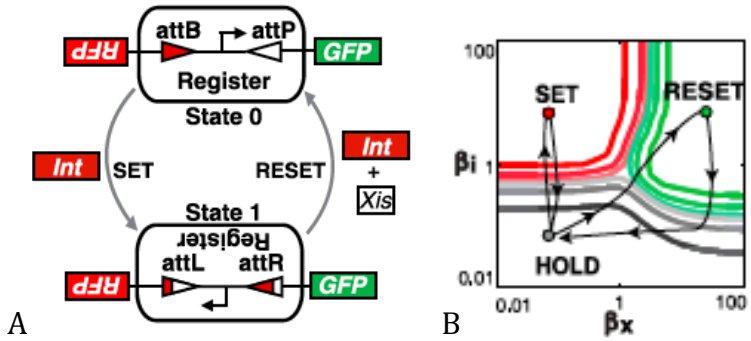

Fig. 3 (A) Architecture and design oft he RAD module (B) Phase diagram showing the three operating regions oft he RAD. β_i presents relative amount of integrase, β_x shows relative amount of excisionase. Published by Bonnet et al 2012.

The RAD module is based on a two state latch design that is able to switch between two different states, as a response to a specific input. Contrary to recently described systems, the RAD module is able to hold the latest state, even in absence of an input. This state is stably imprinted in the chromosomal DNA of the bacterium and gets inherited to the next generation (Fig. 7). The RAD module is based on the natural recombination system of the bacteriophage Bxb1. This phage uses a serine integrase integration system of the Bxb1 genome into the chromosome of host bacteria, naturally *Mycobacterium smegmatis*. Temperate bacteriophages use integrase and excisionase for a site-specific recombination between the infecting phage chromosome (attP) and the specific site of the bacteria host chromosome (attB). This state is called BP. After the integration event, new sites attL and attR are generated. This state is called LR. At the transition of lysogenic to lytic growth of the bacteriophage, integrase and excisionase are expressed to restore the phage genome and the attB and the attP sites, so that the chromosomal DNA remains in the BP state. Importantly, Bbxb1 integrase-excisionase system belongs to the serine recombinase family, which does not require any host cofactors. This makes the system easier to transfer to different hosts.

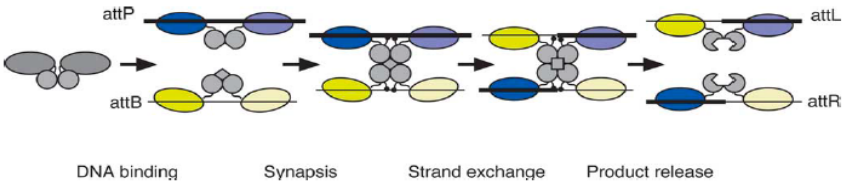

Fig. 4 Schematic model of the recombination of the Bxb1 integration. Unbound integrase dimer (id) is shown left handed in grey. After two ids bind to attP (blue) or attB (yellow), they form a tetramer. This leads to a strand exchange followed by the product release (Ghosh, Pannunzio et al. 2005).

Bacteriophage Bxb1 has a well-characterized integrase-excisionase system. Minimal sites for attB, attP, attL and attR have been described. Gosh and coworkers (Ghosh, Pannunzio et al. 2005) proposed from biochemical in vitro experiments that integrase binds as a dimer to attB as well as another integrase dimer to the attP site. Both bind with their C-terminal domain to a specific sequence of the DNA. This binding causes a conformational change of the dimer, so that the N-terminal catalytic domain is then able to form an integrase tetramer while the dimers are still bound to the DNA. Cleavage occurs by double strand break and strand exchange takes place through a subunit rotation mechanism (Fig. 4). The products are released as dimer DNA complexes that are then in the LR state. It was shown both in vivo and in vitro that the excisionase controls the recombination directly.

The RAD module, described in Bonnet et al. as an SR-Latch, consists of three parts: the DNA data register, the set and reset generator (Fig. 5A). The DNA data register consists of a constitutive promoter, flanked by the attB and attP sites. The set generator consists of an integrase gene, expressed under the control of an aTc inducible promoter. The reset generator consists of excisionase and integrase bicistrons, which are expressed under the control of an arabinose (ara) inducible promoter.

In the presence of aTc, the activated set generator produces integrase. Consequently the DNA data register, flanked by attB and attP (BP state), will switch to the inverted sequence, flanked by attL and attR (LR state). In the presence of ara, the activated reset generator produces both integrase and excisionase, will restore the DNA data register and the flanked sites to the original orientation and identity.

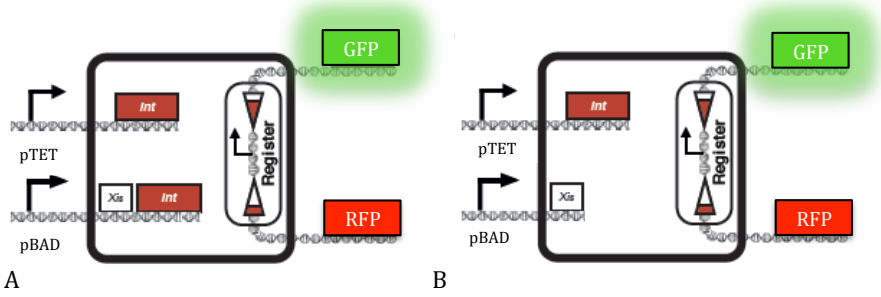

Fig. 5 (A) Published architecture of the RAD called S-R-Latch (B) Alternative architecture of the RAD module, called D-Latch (Bonnet, Subsoontorn et al. 2012)

The D-Latch RAD module used in this project expresses integrase and excisionase under an aTc inducible promoter and an ara inducible promoter, respectively (Fig. 5B). This architecture offers a more convenient possibility for quantitative characterization by independently controlling the amounts of integrase and excisionase by two different inducers.

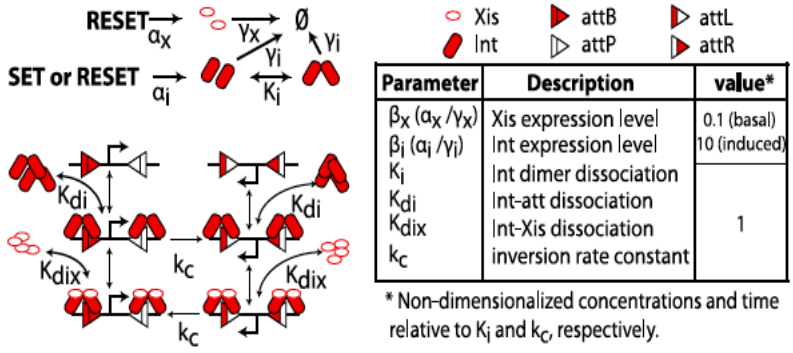

Parameter	Description	value*
β_X (α_X /γ_X)	Xis expression level	0.1 (basal)
β_i (α_i /γ_i)	Int expression level	10 (induced)
K_i	Int dimer dissociation	1
K_{di}	Int-att dissociation	
K_{dix}	Int-Xis dissociation	
k_c	inversion rate constant	

* Non-dimensionalized concentrations and time relative to K_i and k_c, respectively.

Fig. 6 Schematic of the chemical kinetics model of the RAD module (Bonnet, Subsoontorn et al. 2012).

Based on the available information (Ghosh, Kim et al. 2003; Ghosh, Wasil et al. 2006; Ghosh, Bibb et al. 2008), a chemical kinetic model was established for better understanding the behavior of the RAD (Fig. 6). With this model the operating regions were explored.

However, this system needs to be better characterized, so that it can be used as standard biological part for various applications. Hence, my bachelor thesis project was a quantitative characterization of the rewritable addressable data storage module with in silico and in vivo studies. The first part of my bachelor thesis included in silico work. First a teaching model was developed as tool for introducing students and researchers basic mechanisms of RAD module operations. The number of reactions as well as the number of species was reduced, compared to the Bonnet et al. model. However, the model was still capable of simulating the experimentally observed behaviors. The model was used to answer how the output of the RAD module changes by given different levels of input. The output was described as a fraction of the DNA data register in LR state. The input was described by the amounts of integrase and excisionase. We also used the model to explore how the input-output relationship changed with different initial amounts of the data register in BP and LR states. The second model developed for this work was based on the model described in the Bonnet et al. paper but using more realistic kinetic parameters derived from literature and proved by experimental results. We applied this model to map the behavior of the DNA data register as a heat map that showed the different outputs (flips to the LR-state) at different input levels (amounts of integrase and excisionase).

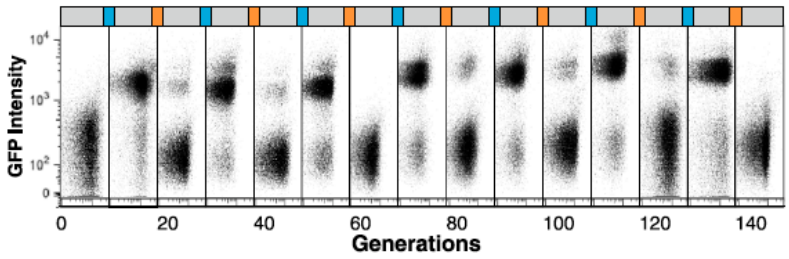

Fig. 7 Multicycle of the RAD module, operation set and reset that show rewritability and stability of the system in terms of operational live time (Bonnet, Subsoontorn et al. 2012).

Experimentally, we developed the following experimental systems to quantitatively explore the input-state relationships of the RAD module. System number 1 was built to map the arabinose concentration in the media to the expression level of the arabinose inducible promoter. The system consisted of a plasmid that had super folding green fluorescent protein under an arabinose inducible promoter (pBAD). We tested it in two strains, DH5alphaZ1 (used in the original RAD module (Bonnet, Subsoontorn et al. 2012)) and BW27786 (linear arabinose inducible promoter (Khlebnikov, Datsenko et al. 2001)). System number 2 was developed to map the aTc concentration in the media to the expression level of the aTc inducible promoter (pTET). The system consisted of a plasmid that had the fast folding green fluorescent protein under pTET in DH5alphaZ1. System number 3 was built to map the switch-threshold of the ara inducible set with respect to the arabinose concentration in the media. The system consisted of integrase expressed under pBAD on a plasmid and the RAD module integrated into the chromosome of DHalphaZ1 and BW27786. System number 4 was built to map the boundaries between set and reset and between reset and hold. The system consisted of integrase expressed under pTET and

of excisionase expressed under pBAD on a plasmid and the RAD module integrated into the chromosome of DH5alpha Z1 and BW27786 with a tetracycline repressor. This system allowed us to fine-tune independently the production rates of integrase and excisionase by adapting the levels of aTc and arabinose in the media. System 3 and 4 were used for mapping the state of the DNA data register to the inducer (ara and aTc) concentration in the media. System 1 and 2 were used for mapping the inducer concentration to the promoter activity. The four systems together allowed us to map the promoter activity to the state of the DNA data register. This project also gave us the possibility to explore how the RAD module, originally optimized for one genetic environment (DH5alphaZ1), behaved in a different genetic environment (BW27786).
However, this experimental design had several intrinsic limitations that prevented a full characterization of the RAD module behavior: (i) the used reporter system was not sensitive enough, (ii) the standard curve of the of the inducible promoters was made for a different protein than integrase and excisionase and (iii) the standard curve was not linked to a fixed standard (e.g. relative promoter units (RPU)).
Because of these drawbacks we wanted to develop another measurement system that used RUP defined promoters. This system would not have any problems concerning the sensitivity of a reporter system. Also this measurement system could be easier reused for characterizations of new RAD modules, as soon as it is established. The used plasmid would consist of an anti-parallel orientated integrase (int) and excisionase (xis) gene cassettes with promoters and RBS in the middle. The two bicistron RBS mirror inverted sites, were synthesized and called GBU1 (included an overlap with int) and GBU2 (included an overlap with xis). The aim was to clone these parts (int, xis, GBU1, GBU2) together on a backbone plasmid (Bb). This design eliminates the transcription read-through problem between integrase and excisionase and also allows us to change, on one DNA piece, the expression control elements, in our case the promoter regions, for both genes. The library of different combinations of standard constitutive promoters was supposed to be synthesized as single stranded parts. After annealing the single bands together, the promoter cassettes should be cloned into the measurement vector. These plasmids should be transformed into DHalphaZ1, which contained the RAD in BP or LR state. The integrase and excisionase would be expressed under the control of the constitutive cloned in promoters. When the expression level would hit the threshold point of the RAD module, we would expect a recombination. We wanted to use the FACS to distinguish in which state (set, reset or hold) the DNA data register was and to sort the bacteria. The sorted bacteria should be regrown. The following step would have been to sequence integrase and excisionase expression controllers of those bacteria. Because we know the sequence of the transformed promoters, after sequencing of the switched cells we could lead back to the promoter combination that was included. We planned to see which promoter combination caused which behavior of the DNA data register (Scheme of work flow see appendix). The advantage of this subproject would be that we could link the recombination events to a standardized input. The main goal was to generate a heat map of the stoichiometric amounts of integrase and excisionase that were needed for recombination. Also this system would have been easy to reuse for future characterization of new RAD systems or controlling sites and could be scaled up and to change the promoter region and the ribosomal binding site. Another application of the system could be to find fast and easy the best combination in a library of different combinations of promoters and ribosomal binding sites to perform a recombination.

2 Material and Methods

2.1 Materials

2.1.1 Machines

Autoclave	Steris, Mentor, USA
Centrifuge Galaxy Mini	VWR, San Dimas, USA
Centrifuge, Mini Spin	Eppendorf, Hauppauge, USA
Coulter Microfuge 18	Beckman, Brea, USA
Coulter Avanti J-E Centrifuge	Beckmann, Brea, USA
Forma Orbital Shoker HEPA Filter 37°C	Thermo Eelctron Corporation, Waltham, USA
Forma Orbital Shoker HEPA Filter 30°C	Thermo Eelctron Corporation, Waltham, USA
Gel visualizer	Bio-Rad, Hercules, USA
Heat Block 37°C/80°C/40°C/46°C	Thermo Scientific Thermolyne, Asheville, USA
High speed centrifuge Avanti J-E high	Beckmann, Brea, USA
Incubator 30°C	VWR, San Dimas, USA
Incubator 37°C	VWR, San Dimas, USA
Inverted microscopes system Axiovert	Zeiss, Peabody, USA
Molecular Imager FX Pro Plus	Bio-Rad, Hercules, USA
NanoDrop ND-1000 Spectrophotometer	Thermo Scientific, Asheville, USA
Plate Reader precisely 1420 Multilabel Counter Victor 3V	PerkinElmer, Boston, USA
Power supply gel chamber PAC 300	Bio-Rad, Hercules, USA
PTC-200 Peltier Thermal Cycler	MJResearch, St. Bruno, Canada
S1000 Thermal Cycler	Bio-Rad, Hercules, USA
Shaker X Lab-Therm LT-X 30C	Kuhner, Birsfelden, Switzerland,
Thermal Cycler	Bioer Technology, Hangzhou,P.R.China
Ultracentrifuge Optima L90	Beckmann, Brea, USA
Vacuum manifold QIAvac 24 Plus	Qiagen, Valencia, USA
Vortexer Mini Vortexer	VWR, San Dimas, USA
Water purification system Milli-Q Advantage A10	Millipore, Billerica, USA
LSRII cytometer	BD-Bioscience, San Jose, USA

2.1.2 Kits and Enzymes

QIAprep® Spin Miniprep Kit (250)	QIAGEN, Valencia, USA
MinElute® Reaction Cleanup Kit	QIAGEN, Valencia, USA
KAPA2G™ Robust PCR Kit	Kapa Biosystems, Boston, USA
Phusion® High-Fidelity DNA Polymerase	New England Biolabs, Ipswich, USA
Platinum® PCR SuperMix High Fidelity	Invitrogen, Carlsbad, USA
Dpn1 Restriction Enzyme	New England Biolabs, Ipswich, USA

2.1.3 Reagents

Glycerol	Fisher Scientific, Hampton, USA
L-Arabinose (ara)	Calbiochem, Darmstadt, Germany
Anhydrotetracycline (aTc)	Sigma, St. Louis, USA
Kanamycin (30µl/ml)	Sigma, St. Louis, USA
Chloramphenicol (25µl/ml)	Sigma, St. Louis, USA
Ampicillin (25µl/ml)	Sigma, St. Louis, USA

2.1.4 Media and Buffer

	LB-plate Media	LB-liquid Media
Bacto-tryptone	10g	10g
yeast extract	5g	5g
NaCl	10g	10g
agar	15g	-
ultra pure H_20	up to 1l	up to 1l

Ingredients were dryly mixed, before water was added and then well mixed. The media were autoclaved at 120°C, 22psi, 30min. Before use we added the required antibiotics.

MOPS EZ Rich Defined Medium Kit. 5 Liter by Teknova

Description	Amount
10X MOPS Mixture	100 mL
0.132 M K_2HP04	10 mL
10X ACGU	100 mL
5X Supplement EZ	200 mL
Sterile H_20*	580 mL
60% Glycerol	10 mL
Total	1000 mL

After mixing the compounds they were sterile filtered and the media was kept at 4°C.

2.1.5 Computer Programs and Web pages

Program name	Company or Webpage	Description
FLOWJO Ver. 8.8.7	Treestar Incuding	Analysis program for FACS data
ApE - A plasmid Editor	Freeware by M. Wayne Davis	Plasmid and DNA Editor
MatLab® Student Version	Mathworks	Basic Simulation and modeling program
The Coli Genetic Stock Center	http://cgsc.biology.yale.edu/index.php	Data Base and Stock Center of E. coli strains
Registry of Standard Biological Parts	http://partsregistry.org/Main_Page	Data Base of Standard Biological Parts

2.1.6 Strains, constructs and oligonucleotides

2.1.6.1 Strains

For the experiments below we used two laboratory strains of non-pathogenic *Escherichia coli*, DH5αZ1 (Hanahan 1983; Lutz and Bujard 1997) and BW27786 (Khlebnikov, Datsenko et al. 2001). The major difference between the two strains was their ara transporter/metabolizer gene cluster. Specifically, while DH5αZ1 had the wild-type ara transporter/metabolizer genes, BW27786 had the following mutations: first, BW27786 had a deletion from -25bp upstream of araB start codon to 8bp in the beginning of araD. AraD and araB were needed for metabolizing ara. For this reason DH5αZ1 could metabolize and therefore change the ara level used in the media as inducer, BW27786 could not metabolize the sugar and was better in terms of holding the arabinose concentration. Second, BW27786 had the deletion of high affinity arabinose transporter, araH-araF, and the replacement of the arabinose-inducible low-affinity arabinose transporter, araE, with araE constitutively expressed. By eliminating the positive feedback between ara induction and ara transporter expression, ara inducible promoters in BW27786 responded linearly to ara concentrations in the media. There were other differences between BW27784 and DH5αZ1 genotypes that may have caused some unknown side effects on the RAD module operations.

Tab. 2 Comparing DH5αZ1 and BW27786 genotypes. The list of mutations compared to the wild type is shown under the strain name. The number in the second line shows the location of the mutation on the chromosome. All information are based on the Yale Escherichia Coli stock center (CGSC) genotype database.

DH5αZ1	BW27786 (Khlebnikov'01)	Comments
	DE(araD-araB)567 1.40	Deletion from -25 upstream of araB start codon to 8bp into the beginning of araD
DE(argF-lac)169 6.21		Deletion from *mmuP* through orfs preceding *argF*, through *lac* to *mhpD*, literally Δ(mmuP-mhpD)169; Omithine carbamoyltransferase mutation, losing ability to utilize arginine
	lacZ4787(del)(:: rrnB3) 7.81	4 tandem copies of the *rrnB* transcriptional terminator inserted by gene replacement into the region extending from near the SacII site near the N-terminus of *lacZ* through the promoter
Φ80dlacZΔM15 8.00		Partial deletion of beta D-galactosidase gene, allowing a complementation of b-galactosidase activity
GlnV44(AS) 14.99		Amber (UAG) suppressor
Lam- 17.40	Lam- 17.40	Lambda lysogen deletion
$Laci^{q}$, PN25-tetR, Sp^{R}		Constitutively producing lacI. Over expression from laciq; Constitutive production of tet repressor expressed from PN25; Spectinomycin resistance at lambda attB site
deoR481 19.00		Regulatory gene mutation allowing constitutive expression of deoxyribose synthesis, allowing large plasmid uptake; grow preferentially on minimal medium with inosine as the sole carbon source.
	DE(araH-araF)570(::FRT) 42.67	Deletion of high affinity ara transporter (encoded by araFGH operon).
gyrA96(NalR) 50.33		DNA gyrase mutation; nalidix acid resistance
recA1 60.80		Missense mutation, altered isoelectric point. Sequenced: G to A for Nuc. 720 (Gly 160 Asp) Prevent HR recombination between host & introduced DNA; UV sensitive
**relA1 62.71		Allow RNA synthesis in the absence of protein synthesis
	araEp-532(del)::FRT 64.20	Deletion of Low affinity ara transporter (encoded by araE)
	$\Phi(P_{CP13}$-araE)534 64.21	Low affinity ara transporter (encoded by araE) is constitutively expressed from P_{CP13} promoter.
endA1 66.57		G to A transition mutation resulting in E208K amino acid substitution; Abolish non-specific endonuclease I activity to improve quality of isolated DNA quality
	DE(rhaD-rhaB)568 88.16	Deletion in rhamnose operon
Thi-1 90.28		Require Thiamine for growth on minimal media
HsdR17(rK-mK+)	HsdR514(rK-mK+) 98.72	Mutation in restriction endonuclease, preventing digestion of foreign DNA.

*described in CGSC but not in Expressys and invitrogen page
** described in Expressys and invitrogen page but not in CGSC

2.1.6.2 Plasmids

All used plasmids were available in the laboratory. None of them was self-designed.

Plasmid #87 (Ara inducible Bxb1 integrase)

This plasmid contained the Bxb1 integrase gene with the sequence of 6 histidine tag near the 5' site of the gene. The gene had a sequence for the degradation tag LAA from ssrA system near the 3' end for increasing integrase degradation rate (Andersen, Sternberg et al. 1998; McGinness, Baker et al. 2006). The integrase gene was under the control of I0500 (pBAD/AraC promoter (from MIT parts registry)). This ara inducible integrase cassette was flanked by a standard biobrick pre- and suffix on pSB3K1 plasmid (p15A ori, 15-20 copies, Kanamycin resistance marker).

Plasmid #1127 (constitutively expressed Tet repressor)

This plasmid had the tetR gene, which was expressed under the control of part J23100 (constitutive promoter from MIT parts registry) and B0034 (strong RBS from MIT). The constitutively expressed tetR cassette was flanked by a standard biobrick prefix and a Pst1 cut site on the pSB4A5 plasmid (pSC101 ori, ~ 5 copies, Ampicillin resistance marker).

Plasmid BBa_J5528 (superfolded GFP under pBAD)
This plasmid contained a superfolded GFP gene (Cambridge iGEM2008). The GFP gene was expressed under the control of 10500 (araC /pBAD from MIT parts registry) and B0034 (strong RBS from MIT parts registry). Downstream from the GFP gene were two terminators B0010 and B0012. The pBAD GFP cassette was flanked by standard biobrick pre- and suffix on the pSB2k3 plasmid (F' ori, <10 copies, Kanamycin resistance marker).

Plasmid SR5A (template for backbone)
The plasmid had a GFP gene flanked by the Biobrick pre- and suffix and two strong terminator sequences upstream of the Biobrick sites. The GFP gene was under the control of a constitutive promoter on the pSB4A5 plasmid (pSC101 ori, ~ 5 copies, Chloramphenicol resistance marker).

Plasmid BBa_I13522 (superfolded GFP under pTet)
This plasmid contained the GFP gene (E0040) expressed under the pTet promoter (R0040) and a strong RBS (B0034). The gene cassette was flanked by standard biobrick pre- and suffix on the pSB1A2 plasmid (pUC19-derived pMB1 ori, 100-300 copies, and Ampicillin resistance marker).

H-3 - DLatch (integrase under pTET and excisionase under pBAD)
This plasmid had the Bxb1 integrase gene expressed under pTET (R0040) and the 6N-RBS (randomized RBS seq.) and the Bxb1 excisionase gene expressed under part I0500 (AraC/pBAD) and the RBS 50000 RBS. The excisionase gene included a sequence of the AAK-tag to destabilize excisionase and thus to reduce interference of the integrase function (Bonnet, Subsoontorn et al. 2012). The B0014 terminator separated the integrase and excisionase gene cassettes. The device was flanked by standard biobrick prefix and suffix on the J64100 plasmid (ColE1ori, 15-20 copies, Chloramphenicol resistance marker).

HK22 helper plasmid (Haldimann and Wanner 2001)
This plasmid had the gene for HK22 integrase. The HK22 integrase gene was expressed under the control of cI857, a temperature sensitive promoter. When a culture containing this plasmid was transferred from 30°C to 37°C the plasmid expressed HK22 integrase transiently and was then eliminated. The HK22 cassette was on the pINT-ts plasmid. This plasmid was temperature sensitive and had to be cultivated at 30°C. The pINT-ts plasmid had three open reading frames: cI repressor, lambda integrase and carried the Ampicillin resistance marker (bla).

Plasmid #1001 (integrase under pTET, excisionase under pBAD)
The plasmid contained the integrase and the excisionase genes. The Bxb1 integrase gene was under the control of ATc inducible pTET promoter and the randomized RBS designed by Jerome Bonnet. The excisionase gene was under the control of the ara inducible pBAD promoter and B0034 RBS. Both genes included the sequence of 6 his-tags at the N-terminus. The standard biobrick pre- and suffix flanked the whole cassette. The cassette was cloned into the pSB3K1 plasmid (p15a ori, 10-12 copies, Kanamycin resistance maker).

Φ80helper plasmid (Haldimann and Wanner 2001)
This plasmid contained the gene for Φ80 integrase under the control of cI857, a temperature sensitive promoter. When a culture containing this plasmid was moved from 30°C to 37°C the plasmid expressed Φ80 integrase transiently and was then eliminated. The Φ80 cassette was on the pINT-ts plasmid. This plasmid was temperature sensitive and had to be cultivated at 30°C. The pINT-ts plasmid had three open reading frames: cI repressor, lambda integrase and carried the Ampicillin resistance maker.

FSP20 (helper plasmid containing Φ21 integrase)
This plasmid had the pAh121 gene (Φ21 integrase gene) under the expression control of a temperature sensitive promoter. Therefore bacteria containing this plasmid had to be cultivated at 30°C. The plasmid contained the Ampicillin resistance cassette. There are no further information about the origin of replication and specific RBSs available.

FSP21 (helper plasmid containing p186 integrase)
This plasmid contained the p186 integrase gene under the expression control of a temperature sensitive promoter. Therefore bacteria that contained this plasmid had to be cultivated at 30°C. The plasmid had the Ampicillin resistance cassette. There were no further information about the origin of replication and specific RBSs available.

FSP43 (integration site 186 and tet repressor)
This plasmid had the 186 integration site and the tetR gene cassette. The plasmid contained the tetracycline resistance cassette. There were no further information about origin of replication and specific RBSs available.

FSP47 (integration site Φ21 and tet repressor)
This plasmid contained the Φ21 integration site and the tetR gene cassette. The plasmid had the tetracycline resistance cassette. There were no further information about origin of replication and specific RBSs available.

DNA data register – Integration Plasmid (Bonnet, Subsoontorn et al. 2012)
This plasmid contained the J23119 (constitutive promoter from the MIT parts registry) flanked by the BP or LR (depending on the state of the DNA data register) recombination sites. Upstream from the BBa_J23119 was the BBa_J61048 terminator in reverse orientation. Upstream the mKate2 (RFP) gene and downstream the superfolded GFP gene flanked by the DNA data register. Both reporter genes were controlled by strong RBS (BIOFAB pilot C-dog project http://biofab.org/data). The whole cassette was flanked by the standard biobrick prefix and suffix on the modified version CRIM system plasmid. The plasmid had the R6k origin of replication (15 copies on Pir^{+}) and contained the integration site PAH70 for HK022 where the KAN was replaced by CAM and a ccdB suicidal gene was added in the multiple cloning site to facilitate cloning. The plasmid had the gene for Chloramphenicol resistance (CamR) marker or the Kanamycin gene (KanR).

2.1.6.3 Synthesized parts

We ordered two parts from the gene synthesis company Integrated DNA Technologies (IDT). We used the gBlock service that synthesizes fragments up to 500bp. The GBU1 and GBU2 were ordered. The sequences are shown in table 3. The parts were nearly mirrored and consisted of a bicistron and a BsaI cut site. GBU1 had an overlap at 3'site with the reverse integrase gene and GBU2 had an overlap at 5' site with the excisionase gene.

Tab. 3 Sequences oft the synthesized parts

Name	Sequence	Length
GBU1	ATTATCATGACATTAGTGACGCGGGACAGGCGGATGACTACCAGGGCTCTGCCGGCCTGGTGGTGATGGTGATGATGTTTCA TTAGAAAGTCTCCTGTGCATGATTAAGATGTTTCAGTACGAAAATTGCTTTCATTGTTGATCTCCTTTTTAAGTGAACTTGC AGGTGGCGGCCGCCACCTGC	184bp
GBU2	TCCTTTTTAAGTGAACTTGCAGGTGGCGGCCGCCACCTGCGGGCCCAAGTTCACTTAAAAAGGAGATCAACAATGAAAGCAA TTTTCGTACTGAAACATCTTAATCATGCACAGGAGACTTTCTAATGAAACATCATCACCATCACCACCAGACTCAGCGTATC GTCTTTCTACCCGATACTCAGTTGCCTACCTATAAAAATAGG	206bp

2.1.6.4 Primer

new name	template	sequence	information	self de-signed
PN1	Backbone SR5A	CAGCGTGGTCGAACGGCTACACACCGG GATGTCGACCGGCTAACGCAAAAAACC CCGCTTCG	**2.mv	+
PN2	Backbone SR5A	CGGGGTTTTTTCGCCTCTAGAAG	*1.mv	+
PN3	#1001 Integrase	AAAATCCTTAGCTTTCGCTAAGGATGA TTTCTGGAATTCGCGGCCGC	*1.mv	+
PN5	#1001 Integrase	GTTAGCCGGTCGACATCCCG	**2.mv	+
PN6	#1001 Integrase	TCTGGAATTCGCGGCCGCTTCTAGAGG CGAAAAAACCCCGCCGAAGCGGGGTTT TTTGCGTTAGCCGGTCGACATCCCG	*1.mv	+
PN8	Backbone SR5A	CAGAAATCATCCTTAGCGAAAGCTAAG G	*1.mv	+
PN9	#1001 Integrase	ATGAGAGCCCTGGTAGTCATCCG	**2.mv	+
PN10	#1001 Integrase	CACCAGGCCGGCAGAG	*1.mv	+
PN11	#1001 Integrase	GGCCTGGTGGTGATGGTGATGATGTTT CATTAGAAAGTCTCCT	*1.mv	+
PN12	G-Block	CGGTGACGCGGGACAGGCGGATGACTA CCAGGGCTCTCATTAGAAAGTCTCCTG TGCATGATTAAGATG	**2.mv	+
PN13	G-Block	GTGACGCGGGACAGGC	*1.mv	+
PN16	#1001 Integrase	AGGAGACTTTCTAATGAAACATCATCA CCATCACCACCA	*1.mv	+
PN17	#1001 Integrase	AGGAGACTTTCTAATGAAACATCATCA CC	*1.mv	+
PN18	G-Block	GCAACTGAGTATCGGGTAGAAAGACGA TACGCTGAGTCATTAGAAAGTCTCCTG TGCATGATTAAGATG	**2.mv	+
PN19	G-Block	AGGCAACTGAGTATCGGGTAGAAAG	*1.mv	+
PN20	#1001 Excisionase	ATGACTCAGCGTATCGTCTTTCTACC	*1.mv	+
PN21	#1001 Excisionase	AGACTCAGCGTATCGTCTTTCTACC	*1.mv	+
PN22	#1001 Excisionase	TTAGCCGGTGACTTCCCAGAC	**2.mv	+
PN23	#1001 Excisionase	ACTGAGCCTTTCGTTTTATTTGATGCC TGGTTAGCCGGTGACTTCCCAGAC	*1.mv	+
PN24	Backbone SR5A	GTTCACCGTTGACGGCCAGGTCTGGGA AGTCACCGGCTAACCAGGCATCAAATA AAACGAAAGGC	**2.mv	+
PN25	Backbone SR5A	CACCGGCTAACCAGGCATCAAATAAAA CGAAAGGCT	*1.mv	+
BBa_G1005	BioBrick suffix	GTTTCTTCCT GCAGCGGCCG CTACTAGTA	rv primer for BioBrick suf	-
BBa_ G1004	BioBrick prefix	GTTTCTTCGA ATTCGCGGCC GCTTCTAG	fv primer for Bio Brick pre	-
BBa_G001001 VR	BioBrick prefix	ATTACCGCCTTTGAGTGAGC	rv primer for seq. Bio-Brick	-
BBa_G00100 VF2	BioBrick suffix	TGCCACCTGACGTCTAAGAA	fv primer for seq. Bio-Brick	-
HK22 VP1	HK22 integration site	GGAATCAATGCCTGAGTG	Verification of integra-tion	-
HK22 VP2	HK22 integration site	GGCATCAACAGCACATTC	Verification of integra-tion	-
Φ80 VP1	Φ80 integration site	CTGCTTGTGGTGGTGAAT	Verification of integra-tion	-
Φ80 VP2	Φ80 integration site	TAAGGCAAGACGATCAGG	Verification of integra-tion	-

*1.mv: first measurement vector design **2.mv: second measurement vector design

2.2 Methods

2.2.1 In silico methods

2.2.1.1 A simplified computational teaching model of integrase/excisionase mediated DNA recombination

Our teaching model was built upon the following assumptions:

1. All chemical reactions followed deterministic mass action kinetic assumptions.

2. The total amounts of integrase, excisionase and DNA data register were constant. Thus, we did not include production, dilution or degradation rates of any chemical species.
3. Integrase and excisionase bound as monomers to the DNA data register and catalyze recombination.
4. There was no interaction between integrase and excisionase in the cytoplasm.

The chemical reactions were converted into ordinary differential equations and numerically solved using MATLAB® ode23s solver.

2.2.1.2 A quantitative computational model of the RAD module using realistic reaction rates

The realistic reaction rate model of the RAD module (rRAD model) was built upon the following assumptions:

1. All reactions followed deterministic mass action kinetic assumptions, like the teaching and the Bonnet et al.'s model.
2. Integrase bound to a recombination site as dimers; a dimer on both recombination sites (forming a tetramer complex) was required for recombination to happen.
3. Integrase and excisionase were not interacting in the cytoplasm.
4. Since the production rates for integrase and excisionase were unknown, we assumed that the default production rate for both was 1nM/min based on the following: first, promoter clearance rate was maximal at 1/second (60 bases/second was the RNA polymerases' speed on approximately 60 base pair long promoters). Second, based on Arkin (Arkin, Ross et al. 1998), we assumed that about 10mM/s were produced per mRNA transcript. With these assumptions we came to the conclusion that the transcription rate per gene was up to 600 molecules (nM) per minute. However, in our case, we used weak RBS and gtg-start codons and suboptimal promoters. Therefore, our production rate was lower. For simplification we assumed a production rate of 1AU/min.
5. The degradation and dilution rates of integrase and excisionase were unknown but assumed to be 0.1mM/min. This assumption was based on the knowledge that protein degradation and dilution rate depended on protein stability and rate of cell growth, respectively. The minimal protein level came down by cell growth and division. Given a typical *E.coli* cell cycle of 20 min, the degradation/dilution was at least log(2)/20nM/s/min ~0.03nM/min. With active degradation, protein half life could go down to a minute (McGinness, Baker et al. 2006) hence the degradation and dilution rates could be log(2)/1 ~ 1mM/min. For our assumption we chose an intermediate rate.
6. The rate of biomolecular reactions depended on the diffusion of the reaction partners and how often they collided. The faster molecules could diffuse, the faster reactions could take place. We assumed that all biomolecular reaction rates were diffusion limited and thus approximately equal to 1nM/min.
7. For the binding affinity of integrase dimers to the recombination sites it was assumed to be 30nM. This assumption was based on the Ghosh et al. 2005 dissociation equilibrium constant for the integrase dimers. The attB or attP sites were 70nM and integrase dimers and attL or attR sites were 15nM. We estimated this dissociation equilibrium between recombination sites and integrase dimers (K_{di}) at 30nM (~average K_{di}). We further assumed that this was constant for all bindings of integrase to any recombination site.
8. For the protein-protein binding reactions like the dimerization of integrases and the binding reactions of excisionases to the BPI2 and BPI4 complexes, we assumed a Kdi of 10nM, a typical dimerization equilibrium constant for protein-protein interactions (Buchler, Gerland et al. 2005).
9. Given that diffusion limited binding rates and estimated dissociation equilibrium constants above, we estimated dissociation rates to be the product of the biding rate and the dissociation equilibrium constant.
10. The catalytic rates of BP to LR and LR to BP recombinations were unknown. The only recombination catalytic rates we have seen were from Ringrose et al. which showed the catalytic rate of Cre and FLP to be 0.006nM/sec and 0.04nM/sec, respectively (Ringrose, Lounnas et al. 1998) (~0.36nM/min and 2.4nM/min, respectively). We used the average between the two catalytic rates for our model. The assumed recombination catalytic (k_c) rate was in the order of 1nM/min.

11. Unlike the model in Bonnet et al. we did not use quasi-steady-state assumptions of binding-unbinding reactions here.

The chemical reactions were converted into ordinary differential equations and numerically solved using MATLAB® ode23s solver, like for the teaching model.

2.2.2 Experimental methods

2.2.2.1 Cell culture

For solid media we used agarose Lysogeny broth (LB) media with proper antibiotics (see material list). The bacteria on the plates were incubated at 37°C or 30°C, depending on the strain and the containing plasmid (see plasmid and strain list).
For liquid media, we used LB media for regular cultures, for example for making competent cells or for the preparation of a glycerol stock. For induction experiments, we used EZ media. Liquid cultures were incubated at 260 rpm on a shaker at 37°C or 30°C, depending on the strain and the containing plasmid (see plasmid and strain list).

2.2.2.2 Glycerol stock

For long-term strain storage, we mixed 500µl of 60% glycerol with 1ml of liquid culture, and injected the solution into the prepared cryogenic tubes and kept them in a -80°C freezer. To use the glycerol stocks, we restreaked them on a plate with a pipet tip and let them grow over night. Single clones from these plates were then inoculated in liquid media. We kept the glycerol stock frozen on ice during this process.

2.2.2.3 Plasmid purification with QIAprep Miniprep Kit

We isolated and purified plasmids from bacteria with the QIAprep Miniprep Kit® by Qiagen (see kit list). The isolation was performed according the manufacturer's description.

2.2.2.4 Polymerase Chain Reaction (PCR)

PCR was used to amplify all DNA parts used for assembling larger constructs or for verifying assembly of parts. Platinum® PCR SuperMix High Fidelity by Invitrogen was used for all amplifications. The mixture contained anti-Taq DNA polymerase antibody Mg^{2+}, deoxyribonucleotide triphosphates, recombinant Taq DNA polymerase and Pyrococcus species GB-D thermostable polymerase. Standard 50µL PCR reactions contained 48µL of Platinum® PCR SuperMix High Fidelity and 0.5µl primer solution (20µM stock solution). The final concentration of primers in the reaction mix was 0.2µM. The thermo cycler protocol included: 1) 94°C for 1min for DNA denaturation and enzyme activation 2) 94°C for 30 seconds for denaturation 3) 55.0°C for 30sec for primer annealing 4) 68 °C for 1min/1kb PCR product for the amplification. Step 2)-4) were repeated 20-30 times then the tube was cooled down to 4°C. The success of the reaction was assessed by gel electrophoreses.

2.2.2.5 Colony PCR

Colony PCR is a method to verify the presence of a DNA construct within a bacterial colony. In general, primers are designed to bind to a unique area of the introduced DNA so that a band of an expected size on an agarose gel would represent a positive screening result, while the absence of this band would represent an unsuccessful transformation or assembly within that bacterial genome.
For this work an individual colony was picked from an agar plate with a pipet tip. Each colony was resuspended in 10µl ultra pure water. We used the KAPA2G™ Robust PCR Kit for Colony PCR. The reaction volume that we used was 10µl for each reaction. 25µl reaction master mix consisted of: 7.25µl ultra pure water, 0.5µl of 20mM DNA primers, 5µl of 5X KAPA2G Buffer A, 0.5µl dNTP (10nM of each dNTP), 0.25µl of 5units/µl KAPA2G Robust DNA Polymerase. In each PCR tube 9µl of the master mix were added. As a template 0.25µl of diluted bacteria was used and had to be added to the PCR tubes. The PCR protocol in the thermocycler was: 1) 94°C for 5min for release DNA from bacteria and activate the polymerase 2) 94°C for 30sec for DNA denaturation, 3) 55°C for 30 sec for primer annealing 4) 72°C for 30sec/1kb PCR product for the amplification. Step 2)-4) were repeated 20-30 times 5) an additional step of 10min at 72°C. The success of the reaction was assessed with gel electrophoreses.

2.2.2.6 Dpn1- Digestion

We used the dpn1 restriction enzyme to clean our PCR reaction product by selectively digesting methylated plasmid DNA templates and leaving only unmethylated PCR products. We added 1-2µl Dpn1 directly to our PCR product. The thermocycler program included 1.5h incubation at 37°C followed by 20min at 80°C for the inactivation of the dpn1-enzyme. Following the digestion we usually used the PCR Purification Kit by Qiagen.

2.2.2.7 PCR product purification (vacuum manifold)

For the purification we used the QIAquick PCR Purification Kit by Qiagen (see kit list). The purification was performed as the manufacturer recommended.

2.2.2.8 Gel electrophoreses

Gel electrophoresis is a standard method to separate and visualize DNA fragments, according to length and structure of the molecules. The agarose gel was made with 1% agarose and 0.5x TBE buffer. The 0.5x TBE buffer was also used as running buffer. To the melted gel we added 1µl ethidium-bromide that intercalated within the DNA and became visible under the UV-light. As a ladder we used 2log by New England Biolab. Before we loaded the sample, we mixed 1µl sample with 5µl 6x loading buffer. The gel ran at 100V for 1h. We visualized the results under UV light with the Biorad gel visualizer.

2.2.2.9 Gibson Assembly (Gibson 2011)

Gibson assembly is a standard method for scarless assembling multiple DNA pieces. The fragments that should be assembled together with this method need to have an overlap of 40bp. These overlaps were added by PCR. For Gibson assembly, two master mixes were needed. First 5x isothermal reaction mix was made from 3ml of 1M Tris-HCl (pH 7.5), 300µl of 1M MgCl2, 60µl of 100mM dGTP, 60µl of 100mM dATP, 60µl of 100mM dTTP, 60µl of 100mM dCTP, 300µl of 1M DTT, 1.5g PEG-8000, 300µl of 100mM NAD and added ultra pure water up to 6ml. Second the assembly master mix contained 320µl of 5x isothermal reaction mix as used for the assembly PCR master mix. The assembly master mix contained 320µl 5X isothermal master mix, 0.64µl of 10U/µl T5 exonuclease, 20µl 2U/µl Phusion DNA polymerase, 0.16µl of 40 U/µl Taq DNA Ligase balanced with ultra pure water to a final volume of 1.2ml. We added 5µl of DNA fragments to the mixture. The fragments should be used in an equal amount. The fragments that were synthesized by PCR were purified with the PCR purification Kit (Qiagen). The reaction took place at 50°C for 15-60min. After the incubation we transformed, in case of a vector assembly, as described in the transformation protocol. When we assembled two parts to one new piece, we used the assembly product as a template for a PCR reaction.

2.2.2.10 Assembly PCR

We used assembly PCR to assembly two pieces of DNA together. The DNA needed to have at least overlaps of 20bp. Because we used the same primers as we used for Gibson assembly to produce the parts, our fragments had overlaps of 40bp. For assembly PCR we used PCR supermix HiFi platinum Master Mix by Life Technologies. As template, we used equal amounts of fragments. The thermocycler protocol was the same as usual but with an elongation time for the whole piece of 15 cycles. Then we added 1µl of each primer to the reaction. We used the forward primer of one piece and a reverse primer of the other piece. The reaction ran for another 25 cycles. After the reaction was finished, we verified the results with gel electrophoresis.

2.2.2.11 Circular Polymerase Extension Cloning (CPEC)

Circular Polymerase Extension Cloning (Quan and Tian 2009) is an assembly PCR modified for assembling circular DNA. For CPEC as well as for the other assembly methods, overlapping regions between the two assembling parts are required. In our study we had overlaps of 40bp. We used Phusion PCR mix. 50µl master mix consisted of 6µl Phusion HF, 1.6µl dNTP and 0.8µl Phusion Taq polymerase and ultra pure water up to total 50µl. The reaction volume of each CPEC was 15µl. To each prepared tube with 10µl of master mix we added equal amounts of fragments. The CPEC thermocycler protocol included: 1) 98°C for 30sec 2) 10sec 98°C 3) 70°C for 1sec then gradually cooled down to 55°C with a ramp of 0.1C/sec 4) 30min at 55°C 5) 72°C for 2h and 15 min. The cycle started once again with the second step and the cycles were repeated 29 times. After 29 cycles the next step was for 5 min at 72°C. After the reaction was finished,

we directly transformed 5µl of the reaction product into bacteria as explained in the transformation protocol.

2.2.2.12 Chemical competent cells

For DNA transformation we needed to make the bacteria cells of different *E.coli* strains competent for DNA uptake. We diluted the bacteria solution 1:100 in LB liquid media with the proper antibiotics. The final volume of competent cell was 1/10 of the used LB volume. We let the cells regrow for 2h till the OD reached a point between 0.3-0.4. The next step was to centrifuge the culture at 3000rpm for 10min at 4°C. We removed the supernatant. Next we added 1/10 of the original volume TSS buffer to the pellet and resuspended it gently on ice. The aliquots of bacteria were frozen in liquid nitrogen and stored in the -80°C freezer.

2.2.2.13 Transformation

With the transformation we brought DNA, in form of a plasmid, into competent bacteria. For transformation, we added 1µl of purified plasmid to 100µl competent cells. When we made cotransformation we used the same amount of each plasmid, note that each plasmid needed a different selection marker. Note, for plasmids that were made with any assembly method, we added 2-5µl. We gently mixed the suspension. We incubated the mixture on ice for 30min, followed by a heat shock at 42°C for 45sec, storage for additional 2min on ice, then added 250-400µl LB media and incubated it for 1h with constant rotation at 37°C. Note, when the bacteria contained a temperature sensitive plasmid or the transformed plasmid was temperature sensitive, we incubated at 30°C for 2h. Next we plated the cells on LB agar plates with proper antibiotics that were dried and warmed up in the 37°C incubator. Plates were incubated for 12h on 37°C or 30°C depending on the plasmid.

2.2.2.14 Chromosomal integration

Transformation was needed to perform integration to the chromosome (Haldimann and Wanner 2001). Therefore a helper plasmid, that consisted of a specific integrase gene, mostly under the expression control of a temperature inducible promoter, had to be transformed to the cell. Also the plasmid which consisted of the gene cassette that should be integrated to the chromosome, flanked by the specific integration site that matched to the integrase of the helper plasmid, had to be transformed to the same bacteria. Both plasmids could be cotransformed. When the temperature sensitive promoter got activated, integrase got produced and the plasmid with the integration site got integrated to the chromosome. The helper plasmid would leave after the heat activation the cell. The protocol was performed in two steps. First we transformed the HK22 helper plasmid or the Φ80 helper plasmid into the BW27786 strain. Note, that the strains were cultivated on 30°C, because the plasmid had a temperature sensitive origin of replication. The cells containing the helper plasmid (containing HK22 or Φ80 integrase gene) were made chemically competent and transformed with the corresponding integration vector bearing the DNA data register.

2.2.2.15 Induction

For the induction series we used a stock solution of 10% ara and 2mg/ml aTc. We performed the dilution series for the needed concentrations in EZ media. For each experiment we prepared a new dilution series. We added 10µl to each dilution and let them grow over night at 37°C. For all induction experiments, except for the one for the standard linear induction curve, we took 1µl after over night induction and let them regrow for 12h in EZ Media, without any inducer.

For the linear induction experiment with ara we had following concentrations:

0%	$2*10^{-9}$%	$2*10^{-8}$%	$2*10^{-7}$%	$2*10^{-6}$%	$2*10^{-5}$%	$4*10^{-5}$%	$8*10^{-5}$%	$1.6*10^{-5}$%	$3.2*10^{-5}$%	$6.4*10^{-5}$%	$1.28*10^{-5}$%	$2.56*10^{-5}$%	$2*10^{-2}$%	$2*10^{-1}$%

For the linear induction experiment with aTc we had following concentrations:

0ng/ml	0,02ng/ml	0,2ng/ml	2ng/ml	20ng/ml	200ng/ml

For the set and hold experiment :

0%	$2*10^{-9}$%	$2*10^{-8}$%	$2*10^{-7}$%	$2*10^{-6}$%	$2*10^{-5}$%	$4*10^{-5}$%	$8*10^{-5}$%	$1.6*10^{-5}$%	$3.2*10^{-5}$%	$6.4*10^{-5}$%	$1.28*10^{-5}$%	$2.56*10^{-5}$%	$2*10^{-2}$%	$2*10^{-1}$%

For the reset experiment we used the following concentrations of arabinose:

BW27786-H3

0%	00,0005%	0,005%	0,05%	0,5%

DH5αZ1-H3

0%	00,0005%	0,005%	0,05%	0,5%

and with a constant concentration of 20ng/ml of aTc .
For the set-reset experiment we used the following concentrations of aTc and a constant concentration of 0,5% ara.
DH5αZ1-H3:

0ng/ml	0,02ng/ml	0,2ng/ml	2ng/ml	20ng/ml	200ng/ml

2.2.2.16 FACS measurements

Flow cytometer measurements were performed on a LSRII flow cytometer (BD-Bioscience). We used 2.5ml FACS tubes. In each tube we added 1ml filter PBS (filter with 0.2µm filter). To each prepared tube we added 50µl of the liquid cell culture that we wanted to analyze. Short before the measurements took place, we vortexed the samples to make sure that the cell culture suspension was well mixed in PBS. For each data point we measured between 10.000-30.000 cells. For the measurements we used the FIC-A and the PE-Texas-Red laser. We gated according to the control cells that had only chromosomal LR and BP DNA registers. We gated out noise before quantification.

2.2.2.17 Plate reader measurements

For measurements with the plate reader we used the required black plates with transparent ground. Into each well we added 180µl of filtered PBS. The next step was to add 20µl liquid cell culture in each well. For the measurements we used the required GFP filter.

3 Results

3.1 In silico results

3.1.1 A simplified computational teaching model of the RAD

Reaction mechanisms included into the teaching model can be summarized as shown in Fig. 8.

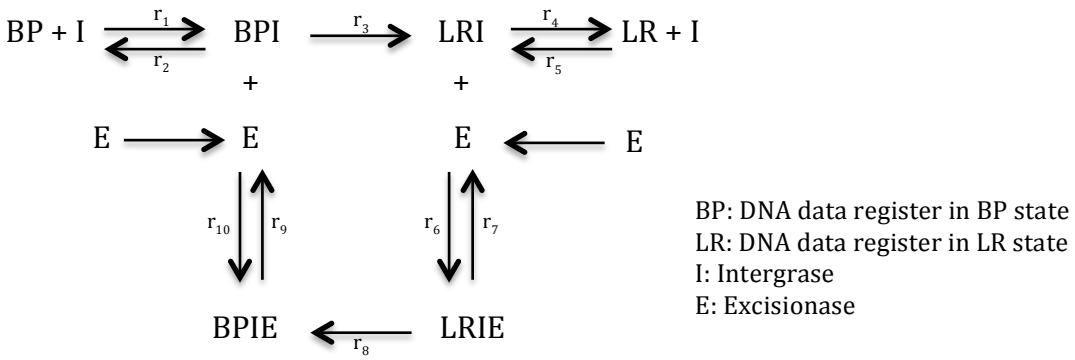

1: BP+I -> BPI
2: BPI -> BP+I
3: BPI -> LRI
4: LRI -> LR + I
5: LR+I -> LRI
6: LRI+E -> LRIE
7: LRIE -> LRI+E
8: LRIE -> BPIE
9: BPIE -> BPI+E
10: BPI+E -> BPIE

Fig. 8 Schematic and elementary chemical reactions used in the teaching model.

The first and the second reaction show integrase associating to and dissociating from the DNA data register in the BP state, respectively. The third reaction shows an integrase-BP state DNA data register complex undergoing recombination to an integrase-LR state data register complex. The fourth and the fifth reaction show integrase dissociating from and associating to the LR state DNA data register, respectively. The sixth and the seventh reaction show excisionase associating to and dissociating from the integrase-LR state DNA data register, respectively. The eight reaction shows an integrase-excisionase-LR state data register complex undergoing recombination to an integrase-excisionase-BP state DNA data register complex. The ninth and the tenth reaction show excisionase dissociating from and associating to the BP state DNA data register, respectively.

Since our goal was to illustrate the qualitative features of the input-output relationship of the RAD module (rather than making precise quantitative prediction), we assumed for simplicity that all reaction rates were equal to one in arbitrary unit.

The chemical reactions were converted into the following differential equations.

```
dy(BP)/dt = r2*BPI-r1*BP*I; - reaction of BP
dy(BPI)/dt = r1*BP*I+r6*BPIE-r2*BPI-r5*BPI*E-r3*BPI;  - reaction of BPI
dy(BPIE)/dt = r5*BPI*E+r9*LRIE-r6*BPIE; - reaction of BPIE
dy(I)/dt = r2*BPI+r4*LRI-r1*BP*I-r10*LR*I; - reaction of I
dy(LRI)/dt = r3*BPI+r8*LRIE+r10*LR*I-r4*LRI-r7*LRI*E; - reaction of LRI
dy(LR)/dt = r4*LRI-r10*LR*I; - reaction of LR
dy(E)/dt = r6*BPIE+r8*LRIE-r7*LRI*E-r5*BPI*E; - reaction of E
dy(LRIE)/dt = r7*LRI*E-r8*LRIE-r9*LRIE; - reaction of LRIE
```

The differential equations were converted into MATLAB readable differential equations (see appendix).

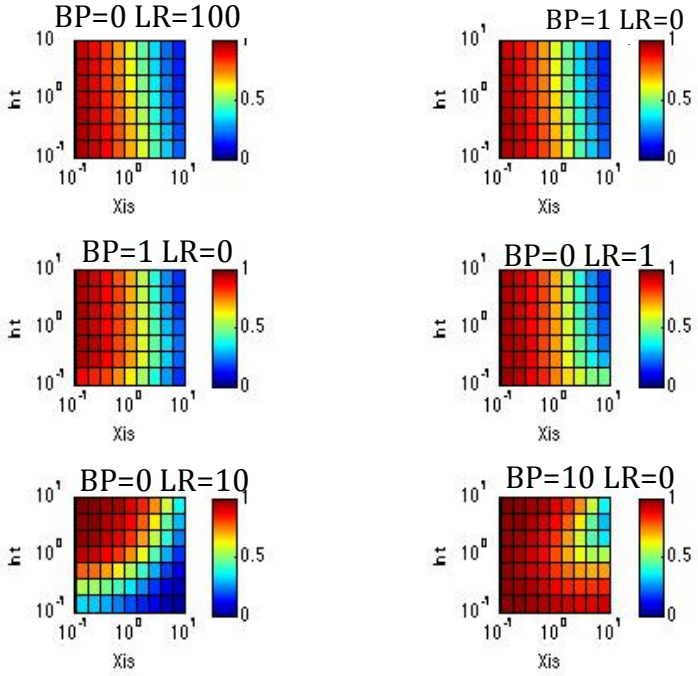

Fig. 9 Simulated phase-diagram showing input-output relationships of the RAD module. For each subplot, the x- and the y-axis showed the amount of excisionase and integrase, respectively. The colors within each phase-diagram represent the RAD output (fraction of LR state data register) ranging from all BP (blue) to all LR (red) after 100 time units of simulation. Subplots in different rows and columns showed input-output relationship given different initial amounts of BP and LR state data register.

The simulated phase-diagram of the RAD module input-output relationship (Fig. 9) showed the following features:

1. When the amount of data register was low (top row), the phase diagrams looked the same, whether we started from all DNA data register in the BP state (top left) or all in the LR state (top right). This feature was expected because when the amount of substrate (DNA data register in BP or LR state) was low, the system reached the steady state quickly. This meant that the final BP or LR fraction did not depend on the initial fraction.
2. As the amount of data register increased (middle and bottom rows), the phase diagram started from all DNA data register in the BP and all DNA data register in the LR became more distinct, especially in the region where total amount of integrase was low (lower part of the phase-diagrams). When the amount of substrate was high, the system was expected to take longer time to reach a steady state, especially when the amount of the catalyst (integrase) was low. Therefore, the final fraction of BP or LR depended on the initial fractions of BP or LR: if the system started with more BP (or more LR), it had more BP (or more LR) at the end of the simulation. We confirmed that the observed dependence of final BP and LR fractions on the initial BP and LR fractions resulted from the fact that the system had yet reached the steady-state by showing with time course simulation that the BP and LR fraction was still changing at time = 100 time units.
3. The final LR fraction depended on excisionase but not integrase, as it can be seen that the boundary between the set (red) and the reset (blue) reached nearly parallel the y-axis, which represented integrase. This behavior is appeared because of we did not include the cooperativity of integrase in this system (Fig. 10).

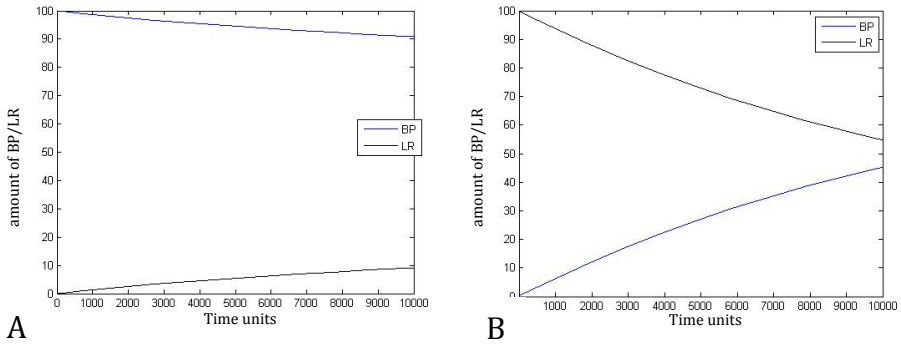

Fig. 10 Time cause kinetic plots of BP and LR. The x-axes show the time and the y-axes show the total amount of BP and LR. Note that the BP and LR levels were still changing at time equal to 100. The initial conditions are for (A) BP=100/LR=0 and for (B) BP=0/LR=100. The two plots correspond to the third row of the heat maps in Fig. 10

3.1.2 Realistic reaction rate model

These are the results of the first quantitative model with realistic reaction rates of the RAD module. For better understanding we show all included reactions (Fig. 6,11).

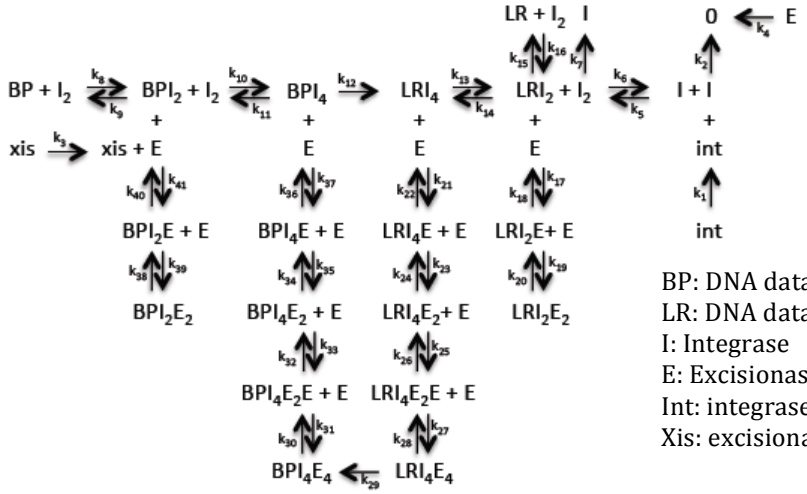

1: int -> int + I
2: I -> 0
3: xis -> xis + E
4: E -> 0
5: I + I -> I2
6: I + I <- I2
7: I2 -> I
8: BP + I2 -> BPI2
9: BP + I2 <- BPI2
10: BPI2 + I2 -> BPI4
11: BPI2 + I2 <- BPI4
12: BPI4 -> LRI4
13: LRI4 -> LRI2 + I2
14: LRI4 <- LRI2 + I2
15: LRI2 -> LR + I2
16: LRI2 <- LR + I2
17: LRI2 + E -> LRI2E
18: LRI2 + E <- LRI2E
19: LRI2E + E -> LRI2E2
20: LRI2E + E <- LRI2E2
21: LRI4 + E -> LRI4E
22: LRI4 + E <- LRI2E
23: LRI4E + E -> LRI4E2
24: LRI4E + E <- LRI4E2
25: LRI4E2 + E -> LRI4E2E
26: LRI4E2 + E <- LRI4E2E
27: LRI4E2E + E -> LRI4E4
28: LRI4E2E + E <- LRI4E4
29: LRI4E4 -> BPI4E4
30: BPI4E4 -> BPI4E2E + E
31: BPI4E4 <- BPI4E2E + E
32: BPI4E2E -> BPI4E2 + E
33: BPI4E2E <- BPI4E2 + E
34: BPI4E2 -> BPI4E + E
35: BPI4E2<- BPI4E + E
36: BPI4E -> BPI4 + E
37: BPI4E <- BPI4 + E
38: BPI2E2 -> BPI2E + E
39: BPI2E2 <- BPI2E + E
40: BPI2E -> BPI2 + E
41: BPI2E <- BPI2 + E

Fig. 11 Schematic and reations that were used for the realistic reaction rate model of the RAD.

The first and the second reaction show the production and the degradation of integrase. The third and fourth reaction show the production and the degradation of excisionase. The fifth and sixth reaction show the dimerization and dissociation of integrase. The seventh reaction shows the degradation of integrase molecules directly from dimers. The eight and ninth reaction show the integrase dimer associating to and dissociating from the BP state data register, respectively. The tenth and eleventh reaction show the second integrase dimer associating to and dissociating from the BP integrase-dimer complex. The twelfth reaction shows an integrase-tetramer-BP state data register complex undergoing recombination to an integrase-tetramer-LR state data register complex. The thirteenth and fourteenth reaction show the integrase dimer associating to and dissociating from the LR integrase-dimer-complex. The fifteenth and sixteenth reaction show the integrase dimer associating to and dissociating from the LR. The seventeenth to forty-

first reaction show excisionase monomers associating to or dissociating from integrase on the recombination sites. The binding stoichiometry between integrase and excisionase is unknown but was assumed to be one-to-one. Thus, up to two excisionase monomers could bind to each integrase dimer on a recombination site.

We converted the chemical reactions above into the following ordinary differential equations (ODEs):

```
dy(BP)/dt = k2*BPI + k12*BPI2 - k1*BP*I - k11*BP*I2
dy(BPI2)/dt = k3*BPI*I - k4*BPI2 - k5*BPI2*I + k6*BPI2 + k11*BP*I2 - k12*BPI2 -
              k13*BPI2*I2 + k14*BPI2I2 + k64*BPI2E -k65*BPI2*E
dy(BPI4)/dt = k7*BPI2I*I - k8*BPI2I2 + k13*BPI2*I2 - k14*BPI2I2 - k15*BPI2I2 +
              k54*BPI2I2E - k55*BPI2I2*E
dy(LR)/dt = k22*LRI2 - k23*LR*I2 + k26*LRI - k27*LR*I
dy(LRI2)/dt = k16*LRI2I2 -k17*LRI2*I2 + k20*LRI2I - k21*LRI2*I - k22*LRI2 + k23*LR*I2
              - k24*LRI2 + k25*LRI*I - k30*LRI2*E + k31*LRI2E;
dy(LRI4)/dt = k15*BPI2I2 - k16*LRI2I2 + k17*LRI2*I2 - k18*LRI2I2 + k19*LRI2I*I
                  - k39*LRI2I2*E + k40*LRI2I2E;
dy(LRI2E)/dt = k30*LRI2*E -k31*LRI2E -k32*LRI2E*E + k33*LRI2E2;
dy(LRI2E2)/dt = k32*LRI2E*E - k33*LRI2E2;
dy(LRI2IE2)/dt = k36*LRI2IE*E - k37*LRI2IE2 -k38*LRI2IE2*E + k70*LRI2IE2E;
dy(LRI4E)/dt = k39*LRI2I2*E - k40*LRI2I2E - k41*LRI2I2E*E + k42*LRI2I2E2;
dy(LRI4E2) = k41*LRI2I2E*E - k42*LRI2I2E2 - k43*LRI2I2E2*E + k44*LRI2I2E2E;
dy(LRI4E2) = k43*LRI2I2E2*E  - k44*LRI2I2E2E - k45*LRI2I2E2E*E + k46*LRI2I2E2E2;
dy(LRI4E4) = k45*LRI2I2E2E*E-k46*LRI2I2E2E2 - k47*LRI2I2E2E2;
dy(BPI4E4) = k47*LRI2I2E2E2 - k48*BPI2I2E2E2 + k49*BPI2I2E2E*E;
dy(BPI4E2E) = k48*BPI2I2E2E2 - k49*BPI2I2E2E*E - k50*BPI2I2E2E + k51*BPI2I2E2*E;
dy(BPI4E2) = k50*BPI2I2E2E -k51*BPI2I2E2*E - k52*BPI2I2E2 + k53*BPI2I2E*E;
dy(BPI4E) = k52*BPI2I2E2 -k53*BPI2I2E*E - k54*BPI2I2E + k55*BPI2I2*E; dy(BPI2E) =
             k62*BPI2E2 - k63*BPI2E*E - k64*BPI2E + k65*BPI2*E;
dy(BPI2E2) = -k62*BPI2E2 + k63*BPI2E*E;
dy(I) = -k1*BP*I   + k2*BPI    -k3*BPI*I + k4*BPI2 - k5*BPI2*I + k6*BPI2I  -k7*BPI2I*I +
        k8*BPI2I2 - k9*I*I + 2*k10*I2 + k18*LRI2I2 - k19*LRI2I*I + k20*LRI2I - k21*LRI2*I
       + k24*LRI2 - k25*LRI*I + k26*LRI-k27*LR*I + k68*int -k71*I + k71*I2;
dy(I2) = 0.5*k9*I*I  - k10*I2     - k11*BP*I2  + k12*BPI2 - k13*BPI2*I2 + k14*BPI2I2 +
          k16*LRI2I2 - k17*LRI2*I2 + k22*LRI2 - k23*LR*I2 - k71*I2
```

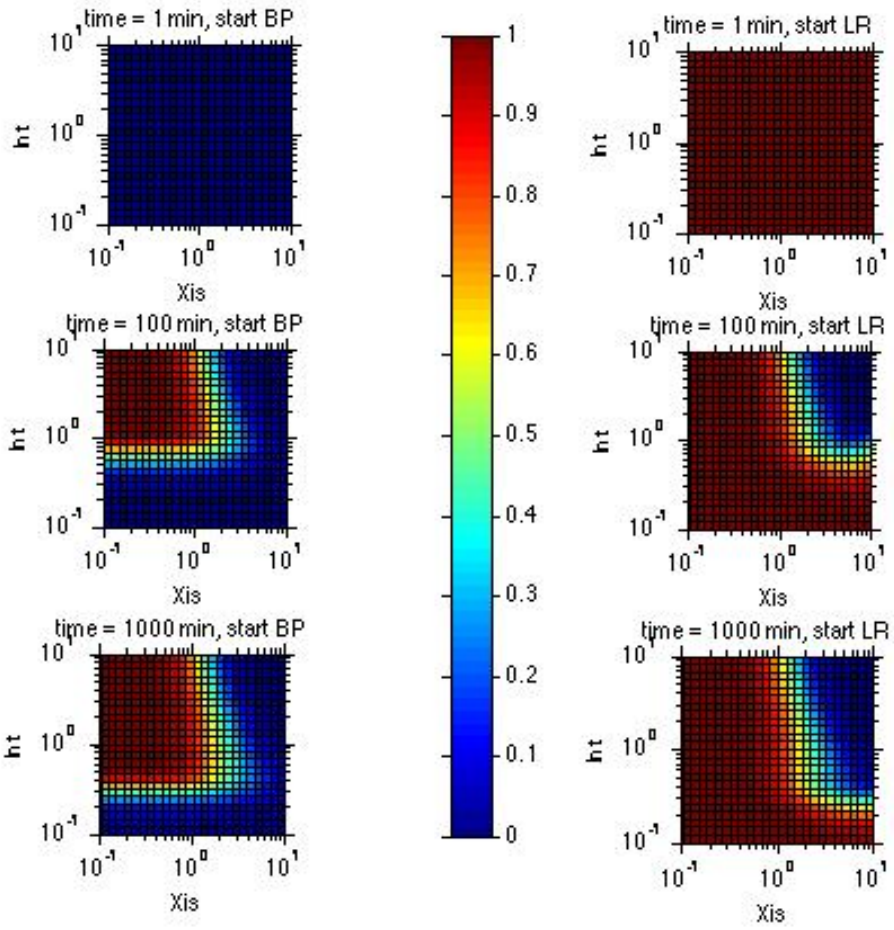

Fig. 12 Simulated phase-diagram showing input-output relationships of a RAD module at different time points. For each subplot, the x- and the y-axis show the production rates of excisionase and integrase in nM, respectively. The colors within each phase-diagram represent the RAD output (measured as the fraction of LR state DNA data register) ranging from all BP (blue) to all LR (red) after 1min, 100min, 1000min of simulation (top middle and button rows). The starting conditions are BP = 1nM, LR = 0nM (left column) and BP = 0nM, LR=1nM (right column).

We used the model with realistic kinetic parameters to explore the three-operation regimes set, reset and hold at different given levels of integrase and excisionase expression rates. In addition, the model could give information of the kinetics of the system. We chose to present the operable range of the expression rates of integrase and excisionase between 10^{-1}nM/min and 10^{1}nM/min, because within this range, all the three behaviors (set, reset and hold) could be captured. The first row of Fig. 12 shows the output after one minute. In the first row there was no change from the starting conditions for any combination of integrase and excisionase expression levels explored. The kinetics of the system were not fast enough to cause any observable switches of the DNA data register. In the next row, we plotted the same starting conditions after 100min. In the region of high amounts of integrase and low amounts of excisionase, the system went to the LR state, regardless where it started. This corresponded to the set region. In the region of high amounts of integrase and high amounts of excisionase, the system went to the BP state, regardless where it started. This corresponded to the reset regime. For low amounts of integrase and low amounts of excisionase, the system remained in the starting condition. This corresponded to the hold regime. The boundary region between the hold and the set state for a simulation of 100min is at 1nM/min integrase. At this point 100% of the DNA data register was in the LR state. The boundary was parallel to the x-axes. The reported boundary region between reset and set started at 1nM/min excisionase. The boundary region between reset and hold was at 1nM/min integrase production rate, and therefore lower than for the set and the hold state. At this point we reported 100% switching of the DNA data register.

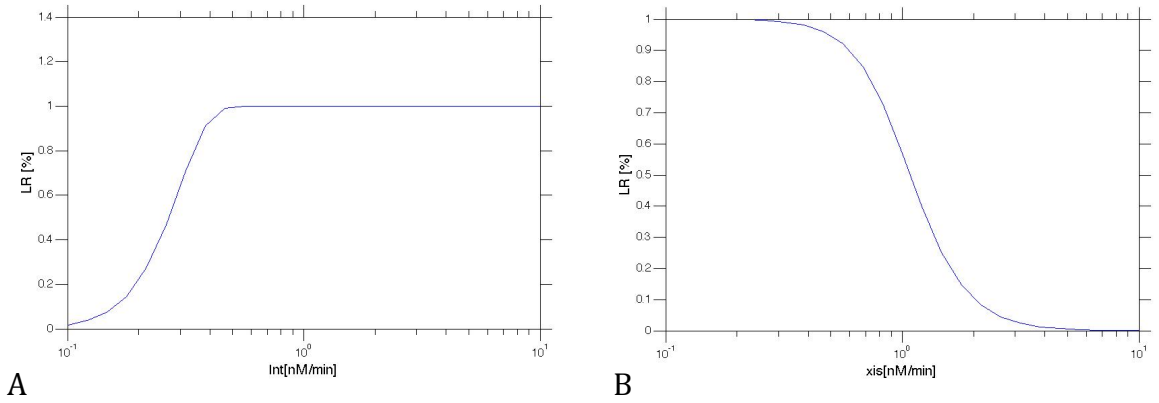

Fig. 13 One dimensional response curves for changing integrase (A) and excisionase (B). The y-axes show the fraction of LR in present. The x-axes show the production rate of Int in nM/min (A) and the production rate of Xis in nM/min (B). With higher production rate of int, more cells were in the LR state (A) while a higher production rate of xis leaded to a switch out of the LR state (B). For the simulation we used the same parameters like we did for the heat map above. The LR fractions were taken form the simulation with 1000 min.

When we plotted the simulation of the states for longer time frames (1000min) the plot did not change much. We still saw a set, reset and a hold state. The boundaries moved towards lower concentrations. The boundaries between set and reset did not change. To visualize the boundary region, we plotted this region also as one dimensional dose response curves (Fig 13). We could see now very clear that the boundary for a total set (more than 99% in LR state) took place at a production rate of 0.5623nM/min of integrase. For a total reset (more than 99% in BP state) the production rate of excisionase had to be at 6.813nM/min. The boundaries between the set or reset and hold state decreased over time towards lower integrase production rates. The speed of decreasing slowed down and nearly stopped around an integrase production rate of 1nM/min. Because of the cooperative behavior of integrase, the system had a switch like behavior. Under a certain threshold, the recombination occurred very slowly. At the lower part of the heat map, the expression rate of integrase was low, if the steady state expression level was below the threshold, the system holded the state for long times.

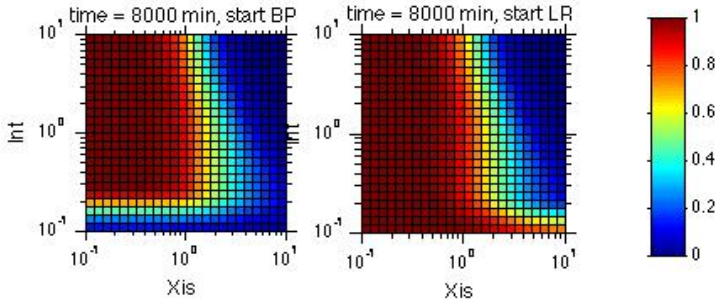

Fig. 14 Simulated phase -diagram input-output relationships of a RAD module after 8000min. For each subplot, the x- and the y-axis show the amount of excisionase and integrase in nM, respectively. The colors within each phase-diagram represent the RAD output (fraction of LR state DNA data register) ranging from all BP (blue) to all LR (red) after 8000 min of simulation. The starting conditions are BP = 1nM, LR = 0nM (left column) and BP = 0nM, LR=1nM (right column).

We assessed the quality of the model by comparing our simulation results to the experimental results of the Bonnet et al. paper. The experiments in the Bonnet et al. paper (Fig. 7) showed, that the system should perform a recombination 4h after induction. Our model showed a similar behavior, as you can see in Fig. 14. Our model could simulate 5 days (7200min) state holding, like observed experimentally.

To test the sensitivity of parameter choices, we increased and decreased each parameter ten fold and compared the results with the experimental behavior of the DNA data register from the Bonnet et al. paper. The first assumption that we tested was the diffusion limited binding rate. For increasing this rate, while keeping all dissociation equilibrium constants, we saw that the system became slow. We could not see any significant switches of the system, even after 1000min. This result did not match with the experimental results of the Bonnet et al. paper (Fig.

4) that showed that a recombination happend in 4h. For decreasing the diffusion limited binding rate, the boundary regions of the three states of the DNA data register became sharper. Especially for the boundary region of the set and reset, there was not shift to higher excisionase production rates, like we reported before. The difference was too small to compare it with the experimental data. The assumed diffusion limited binding rate in our model for was already at the higher end of possible assumptions. However, the rate that we used produced data that were highly comparable to the experimental data in the Bonnet et al. paper.
The next assumption that we tested was the integrase-excisionase dissociation equilibrium constant. When we increased this constant, the switch appeared slower. Also we did not see any reset. This result did also not fit to the experimental data of the Bonnet et al. paper. This could be explained with a higher integrase-excisionase dissociation equilibrium constant. Excisionase did not bind easily to integrase. Both proteins were needed for a reset. However, when we decreased the integrase-excisionase dissociation equilibrium constant, the heat map changed in a way that the set state appeared later. As well the earlier reported shift of the boundary region between set and reset was with this assumption much bigger. However, the reset region was smaller than with our assumptions. These data did not fit to the experimental data of the Bonnet et al. paper. We saw the boundary between set and reset was sensitive to the integrase-excisionase dissociation equilibrium constant. Increasing and decreasing of the degradation rate had a major impact to the behavior of the system. With increasing the degradation, the system lost the ability to perform a reset. The decrease caused the effect of a very fast recombination. The plots for this testing are not shown but can be reproduced with the MatLab codes in the appendix.

3.2 Experimental results

3.2.1 Measurements of the RAD module transfer function using inducible promoters

3.2.1.1 Building of the new chassis BW27786 with a chromosomally integrated DNA data register

We used the method of Haldimann et al. (Haldimann and Wanner 2001)(materials and methods) to integrate and verify the integration of the DNA data register to the chromosome of the BW27786 strain. Integration was confirmed by colony PCR (Fig 15). We subsequently confirmed by microscopy and flow cytometry that chromosomally integrated BP and LR DNA data register expressed detectable amounts of green and red fluorescent proteins, respectively (Fig 16). We also attempted to include the tetracycline repressor expression cassette into BW27786 that included the DNA data register in chromosome or an a plasmid, but without success.

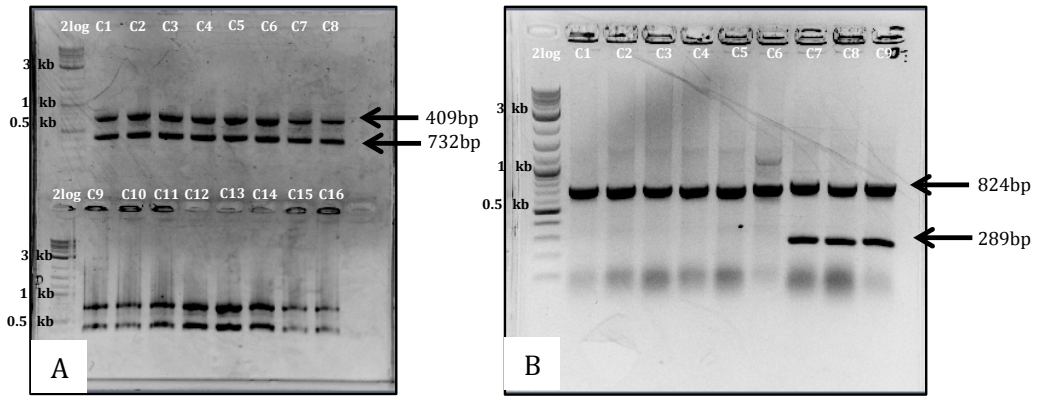

Fig. 15 Data register has been integrated to the chromosome. The gels show the results of a colony PCR of transformed BW27786 that included the DNA data register on a crim integration plasmid. We used the verification primers of Haldimann et al. to prove that the DNA data register was single integrated to the chromosomal DNA. (A) Shows the single integration with Φ80integrase and (B) shows the integration with HK22. Amplification products of the length 289bp and 409bp imply a positive result for the integration at HK22 site; amplification products of a length 409bp and 732bp imply a positive result for the integration at Φ80 site (used verification primer by Haldimann and Wanner 2001). (A) C1to C16 show successful integration of the DNA data register with Φ80 integrase. (B) C7 to C9 show successful integration of the DNA data register with HK22.

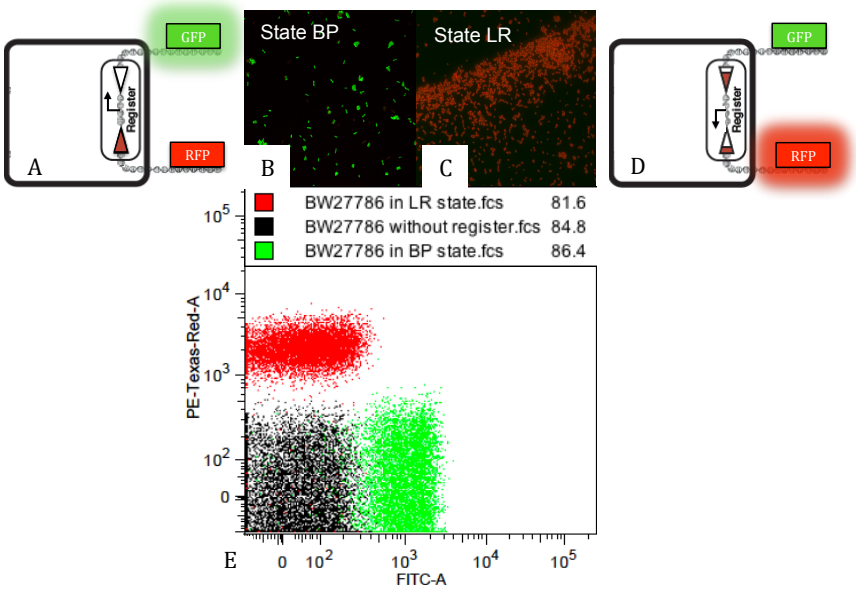

Fig. 16 Chromosomally integrated DNA data register in BW27786 bacteria were visible under the microscope and the flow cytometer. (A,D) show the schematic of the DNA data register in the BP state (A) and LR state (D), (B, C) show fluorescent micrograph of BW27786 in LR (C) or BP state (B). (E) shows flow cytometer plot of cell with a DNA data register flipped in LR (red) or BP (green) state as well as cells without DNA data register (black).

3.2.1.2 Standard curve for arabinose inducible promoter activity in BW27786 and DH5αZ1

For this aim, we transformed a plasmid that contained GFP under the control of pBAD promoter. We compared the response of two different strains, DH5αZ1 and BW27786.

We showed that in BW27786, the arabinose inducible promoter responded linearly to the concentration of arabinose in the media. We used this standard curve to map the concentration of arabinose in the media to the promoter activity. In BW27786, the fluorescent GFP signal, controlled by the arabinose inducible promoter, started increasing linearly at a concentration of arabinose of $4*10^{-5}$%. The linear response of the promoter continued up to an arabinose concentration of $1.28*10^{-3}$%. Above this concentration the expression level saturated.

In the DH5αphaZ1 strain, the fluorescent GFP signal, controlled by the arabinose inducible promoter, started to increase significantly at a $2.56*10^{-3}$% of arabinose concentration in the media. The expression level, shown as a function of arabinose concentration, displayed a switch like behavior.

Single cell fluorescence distribution shown as a histogram confirmed a more linear arabinose induction response in BW27786 than in DH5αZ1. More specifically, we observed in BW27786 unimodal fluorescent distribution gradually shifting towards higher average fluorescence levels when we increased the concentration of arabinose. For DH5αphaZ1, the fluorescence distribution abruptly increased as the arabinose concentration reached a threshold of $2.56*10^{-3}$% (from red to green line, Fig. 17). A different view of the same single cell measurements, a pseudo color plot, showed that BW27786 had nearly a single, homogeneous population of fluorescent cells, whose fluorescence level increased with the concentration of arabinose. Contrary, in DH5αZ1, we observed two separate populations of cells, one presenting low fluorescence, the other one presenting high fluorescence. This effect was particularly notable at intermediate concentrations of arabinose ($6,4*10^{-4}$% to $3,56*10^{-3}$%).

In conclusion, this part of the project allowed us to map the arabinose inducible promoter activity to arabinose concentrations. The observed linear induction response in BW27786 was in agreement with the previous study by Khlebnikov et al. The linear region we presented was in the same region as in the Khlebnikov et al. paper. But we successfully produced a higher resolution map of the linear region of induction.

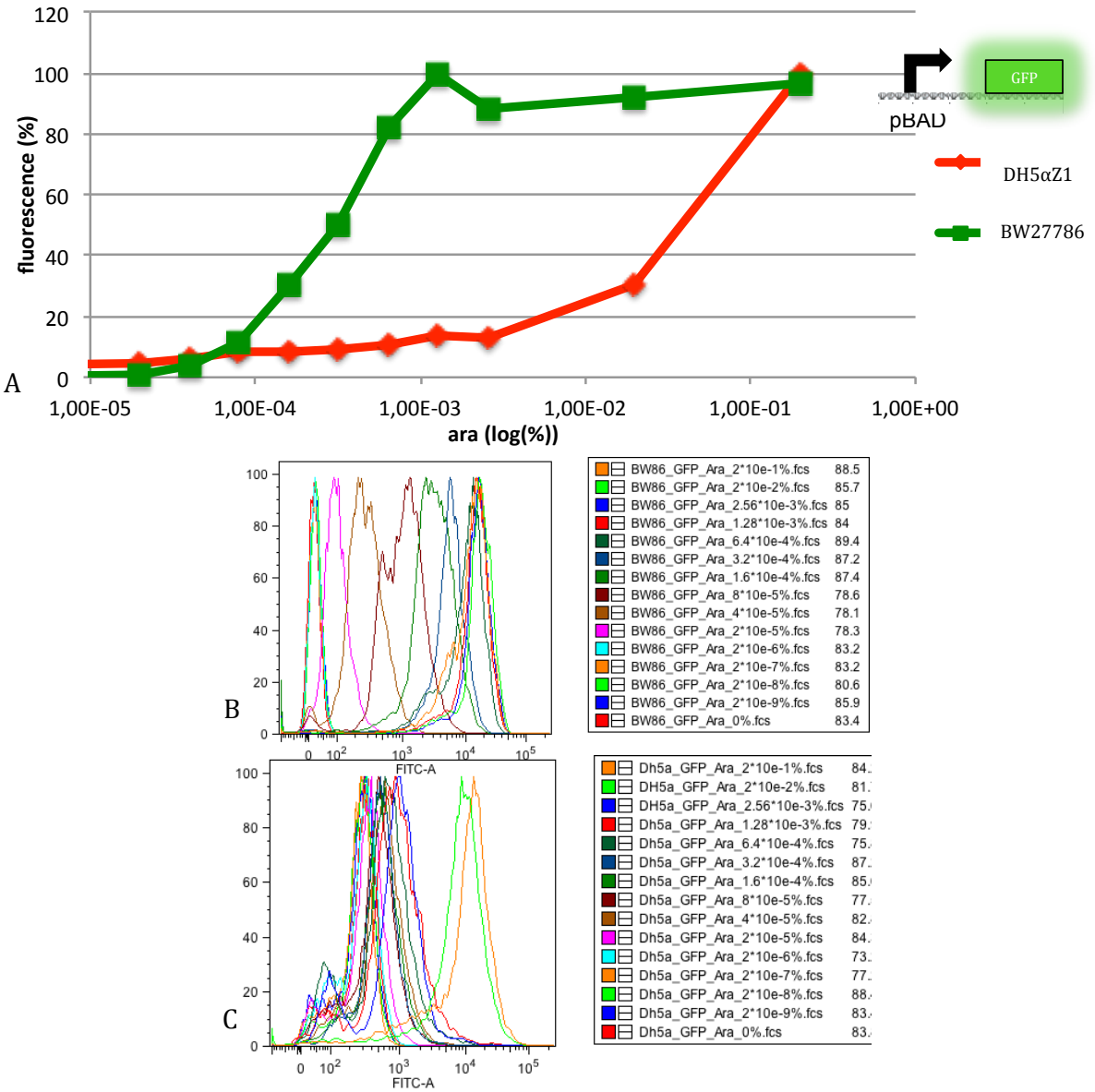

Fig. 17 Input-output response of ara inducible promoter in BW27786 and DH5αZ1. (A) Plate reader results showing the fluorescence intensity of GFP produced by the expressing level of ara inducible promoter in BW27786 (green) and DH5αZ1 (red). The x-axes show the ara concentration in the media in percent, volume in log scale. The y-axes show the GFP fluorescence intensity in percent of the maximum value. Inset shows a schematic of the transformed construct. (B-C) Histogram of BW27786 (B) and DH5αZ1 (C) Different colors correspond to cells induced with different ara concentrations. The x-axes show the GFP fluorescence intensity measured in the FITC-A channel. The y-axes show the percentage of total cell. (D-E) Flow cytometer showing pseudo color single cell fluorescence distribution. Population distribution GFP level (y-axis) and forward scatter (x-axis) levels are shown for samples induced with different ara concentrations for BW27786 (D) and DH5αZ1 (E). All data were generated with three different clones measured for three times. FACS results show linear region for ara is between $8*10^{-5}$% and $1.28*10^{-3}$% similar to the plate reader results.

3.2.1.3 Standard curve for anhydrotetracycline (aTc) inducible promoter activity in DH5αZ1

We mapped the concentration of aTc in the media to the level of gene expression of an aTc inducible promoter (pTET) in DH5αZ1. Therefore we transformed a plasmid that contained GFP under the control of a pTET promoter. In DH5αZ1, the fluorescence signal of GFP under the control of the tetracycline promoter started to increase significantly at a 0.2ng/ml of aTc. The expression level saturated at a concentration level above 20ng/ml of aTc. Single cell fluorescence distribution was obtained by flow cytometry (Fig. 19 B). Single cells showed the same dynamic range expression of GFP under the control of pTET. It showed similar results to the measurements performed in the plate reader for DH5αZ1. A different view of the same single cell fluorescence measurement presented as a pseudo color plot showed that the DH5αZ1 remained nearly as a homogeneous population with increasing fluorescence intensity as aTc concentration increased. We did not have enough data points to claim that the tetracycline inducible promoter

in DH5αZ1 responded linearly to the concentration of aTc in the media. However, our observed range of aTc induction was similar to the dynamic range reported. The study of Lutz and Bujard showed a linear induction range between 1ng/ml and 10 ng/ml in DH5αZ1. We used this standard curve to map the concentration of aTc in the media to the pTET promoter activity.

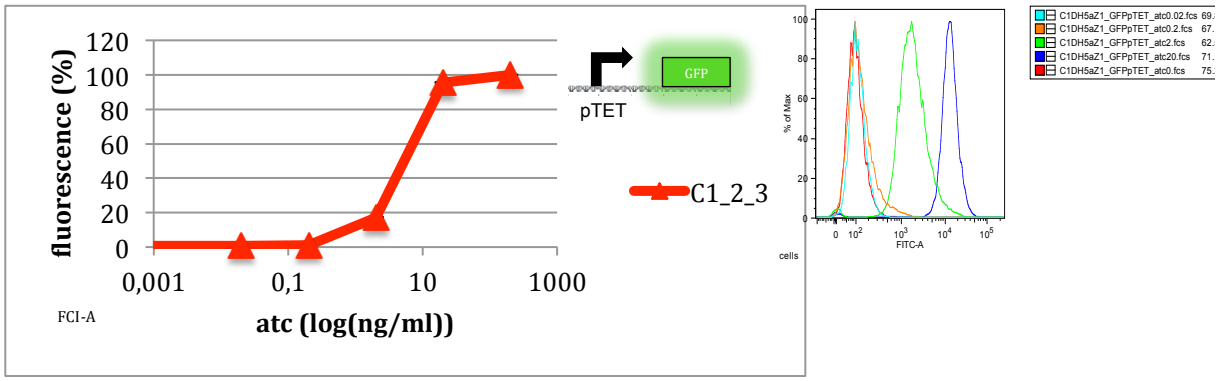

Fig. 18 Input output response of tetracycline inducible promoter DH5αZ1. (A) Plate reader results showing the GFP level expressing of tetracycline inducible promoter DH5αZ1 (red). The x-axis shows the tetracycline concentration in the media in ng/ml in a log scale. The y-axe shows the GFP fluorescence intensity in percent of the maximum value. Inset shows transformed construct. (B) Flow cytometer single cell fluorescents histogram of DH5αZ1 (B). Different colors correspond to cells induced with different tetracycline concentrations. The x-axis shows the GFP fluorescence intensity measured in the FICTC-A chancel. The y-axis shows the percentage of total cell.

3.2.1.4 Arabinose inducible hold-set transition

We used the arabinose inducible integrase to explore the boundary between the hold state and the set state of the RAD module in BW27786 and DH5αZ1. For this aim, we transformed a plasmid, pre-integrated the DNA data register that also contained the integrase gene under the control of pBAD (#87). We started our study with cells that had the DNA data register in the BP state and induced the cells with different arabinose concentrations.

For BW27786 that were grown without arabinose, most of the cells remained in the BP state, except for the third clone, which showed spontaneously a switch to about 60% LR, even without inducer. As we increased the arabinose concentration in the media from $2*10^{-7}$% to $8*10^{-5}$%, the fraction of LR switching to BP gradually increased in three different clones. Above the 8*10-5% arabinose concentration, all three clones switched to the LR state, almost completely. Note that the sum of the BP and LR states from the same culture was not equal to 100%. Possible due to the fact that some cells lost or changed absolute fluorescence expression and thus were not categorized as LR or BP. This may result from mutations of the reporter genes or by mutations of the DNA data register. The threshold point for complete switching was between an arabinose concentration of $4*10^{-5}$% and $8*10^{-5}$%. We observed higher distribution of the cells in the LR fraction than of the BP fraction above the switching threshold ($8*10^{-5}$% arabinose concentration) that all cells were in the BP state. We observed in all colonies that after the switching there was a high number of non-fluorescent cells.

For DH5αZ1, we observed at low arabinose concentrations (below $8*10^{-5}$%) spontaneous switches to the LR state. Note that we observed spontaneous switching of DH5αZ1 was more extreme than in the case of BW27786. Some samples switched nearly complete to LR, while the other remained nearly complete in the BP state. Across the three samples, we found complete switching to the LR state at $2*10^{-8}$% arabinose concentration. At arabinose concentrations above $8*10^{-8}$%, the system reliably switched to the LR state in three different clones. We observed a more switch-like behavior at the transition region between the set and the hold region than in BW27786. We observed for DH5αZ1 in all colonies that after the switching there was a higher number of non-fluorescent cells than in BW27786.

When we compared the arabinose inducible set results (Fig 20A, B) with the standard arabinose induction curve (Fig. 18A), we saw that the transition region between set and hold was at the arabinose concentration that corresponded to 10% of the maximal transcriptional activity of the arabinose inducible promoter.

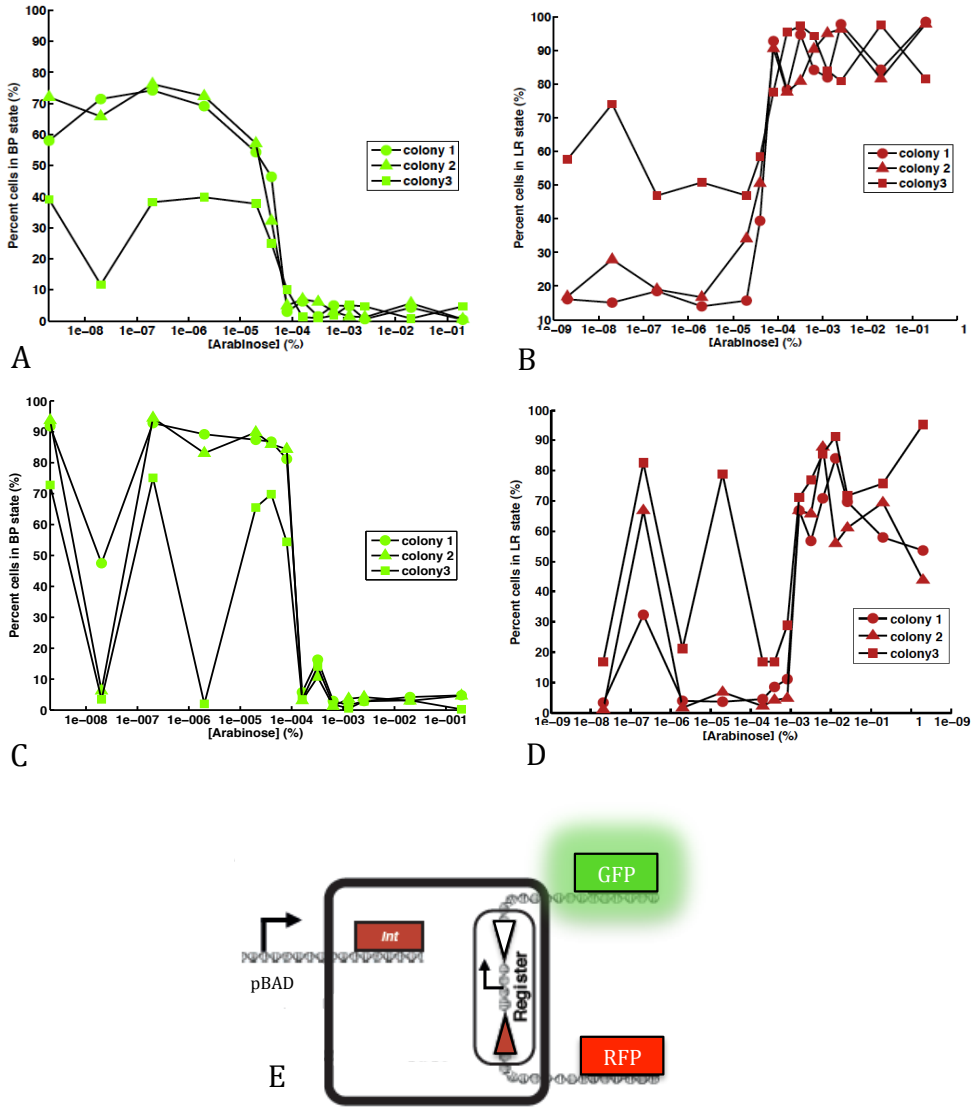

Fig. 19 (A and B) Input state dose response of ara induced integrase from #87 set switch in BW27786 shown as flow cytometry measurements. Fraction of BP state (A) and LR state (B) under different amounts of ara concentration. The three clones used in A were the same used in B. The x-axes show ara concentration in volume percent in log scale. The y-axes show the percentage of cells in BP (green) or LR (red) state. Each data point represents a flow cytometer measurement of induced cells. (C and D) Input-state dose respond of ara induced set switch for DH5αZ1 for similar experiment. (E) shows schematic of the RAD module in the initial condition.

3.2.1.5 Ara inducible set-reset transition

We next used a D-latch plasmid (H3) that we transformed into DH5αZ1 and BW27786. They contained the chromosomally integrated DNA data register. The D-latch consisted of the integrase gene under the control of a pTET promoter and the excisionase gene under the control of a pBAD promoter (D-Latch design and plasmid see material). By independently varying the expression levels of integrase and excisionase, the Dlatch allowed us to explore the boundaries between the set and the reset state for BW27786 and DH5αZ1. Since BW27786 did not have a tet repressor, integrase was constitutively expressed. On the other hand, DH5αphlaZ1 had a tet repressor, so pTET promoter had to be induced by aTc to be active.

We started with cells with the DNA data register in the LR state. For BW27768, we varied the concentration of arabinose in the media and measured the fraction of cells that switched to the BP state.

The threshold for complete switching was at least at 0.0005% arabinose concentration. Since we did not have data points between 0% and 0.0005% arabinose concentration, we could not claim the switch like behavior, nevertheless the transition between LR and BP state was extremely abrupt.

In the DH5αZ1 strain, we kept the aTc concentration at 20ng/ml constant to induce the expression of integrase. We varied the arabinose concentration the same way we did for BW27786.
Below an arabinose concentration of 0.0005%, we observe nearly no switch to the BP state. This behavior matched to the results of the standard curve for DH5αZ1, that showed that a higher arabinose concentration was required to activate the pBAD promoter in DH5αZ1 than in BW27786. Above an arabinose concentration of 0.0005% we observed a switch like behavior. At an arabinose concentration of 0.05% the system reached saturation.
When we compared the arabinose inducible set to reset transition results (Fig. 21) with the standard arabinose induction curve (Fig. 20A), we found that the transition region between reset and hold was at the arabinose concentration that corresponded to 20% expression level of the arabinose inducible promoter. The switch like behavior at the set to reset boundary could either be the result of: (i) the switch like behavior of the arabinose induction for excisionase expression and/or (ii) the switch like behavior of excisionase controlled recombination.

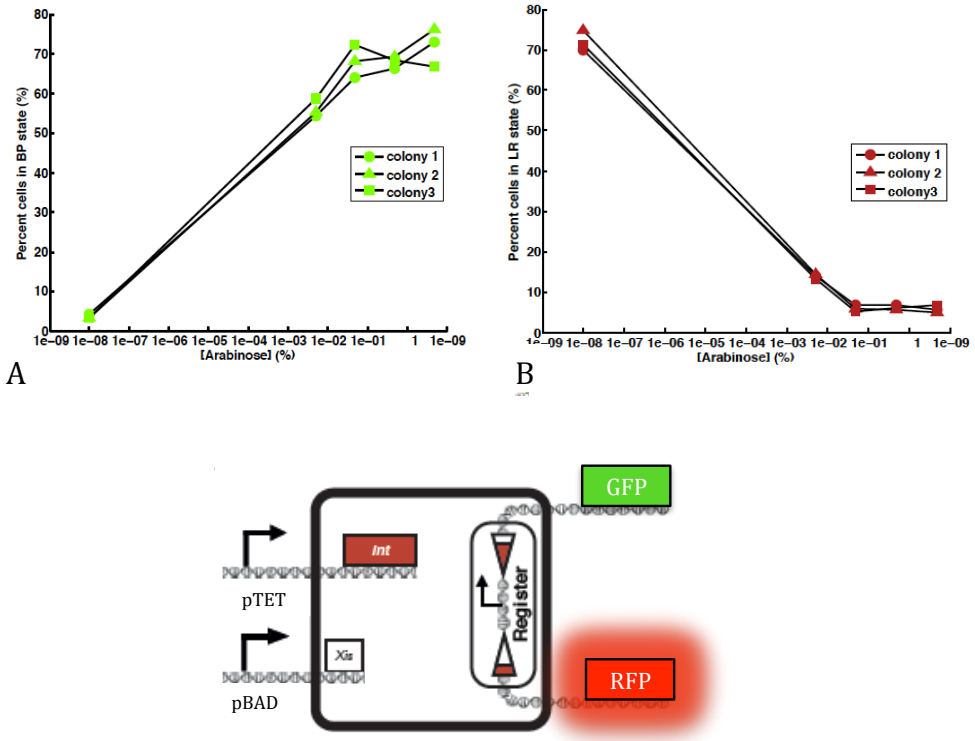

Fig. 20 (A and B) Input state dose response of ara induced excisionase from H3-Dlatch in BW27786 measured with the flow cytometer. Integrase was expressed under a tetracycline promoter, which was constitutively expressed due to the absence of the tet repressor. We show the fraction of BP state (A) and LR state (B) under different ara concentrations. The three clones used in (A) are the same used in (B). The x-axes show the ara concentration in volume percent on a log scale. The y-axes show the percentage of cells in BP (green) or LR (red) state. (C) shows schematic of the RAD module in the initial condition.

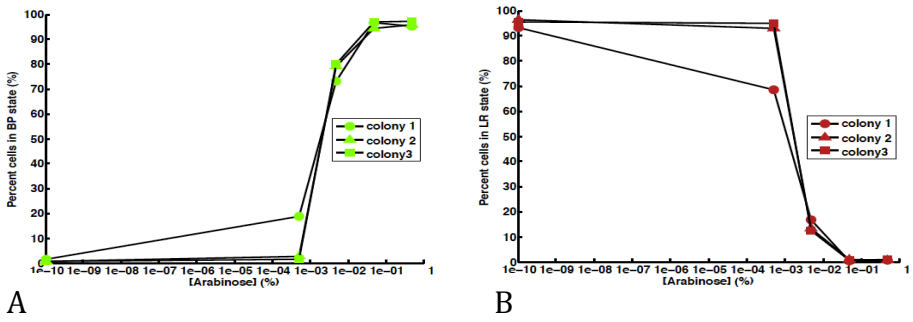

Fig. 21 (A and B) Input state dose response of ara induced excisionase from H3 D-latch in DH5αZ1 measured with the flow cytometer. Integrase was expressed under the control of a tetracycline promoter, induced with a fixed aTc concentration (20ng/ml). We showed the fraction of BP state (A) and LR state (B) under different ara concentrations. The three clones used in (A) were the same used in (B.) The x-axes show the ara concentration in volume percent on a log scale. The y-axes show the percentage of cells in BP (green) or LR (red) state. See Fig 20 (C) for RAD module in initial condition.

3.2.1.6 Anhydrotetracycline inducible reset-hold transition

We used H3 D-latches that we transformed in DH5αZ1 that contained the chromosomally integrated DNA data register, with integrase under the control of a pTET promoter and excisionase under the control of a pBAD promoter (D-Latch design and plasmid see material) to explore the boundary between the reset and the hold state for DH5αZ1.

We kept the arabinose concentration at 0.5% constant to induce excisionase, but we varied the aTc concentration from 0ng/ml to 0.2ng/ml to 2ng/ml to 20ng/ml and to 200ng/ml.

We observed a switch like transition at an aTc concentration above 2ng/ml. Below this threshold, we observed nearly no switch to the LR state. Above a concentration of 20ng/ml the system reached saturation. Note, that the reset to hold transition region matched the transition region of the standard curve of aTc induction in DH5αZ1.

This reset to hold transition regime was not fully explored in this work since expressing the tet repressor in BW27786 was not possible.

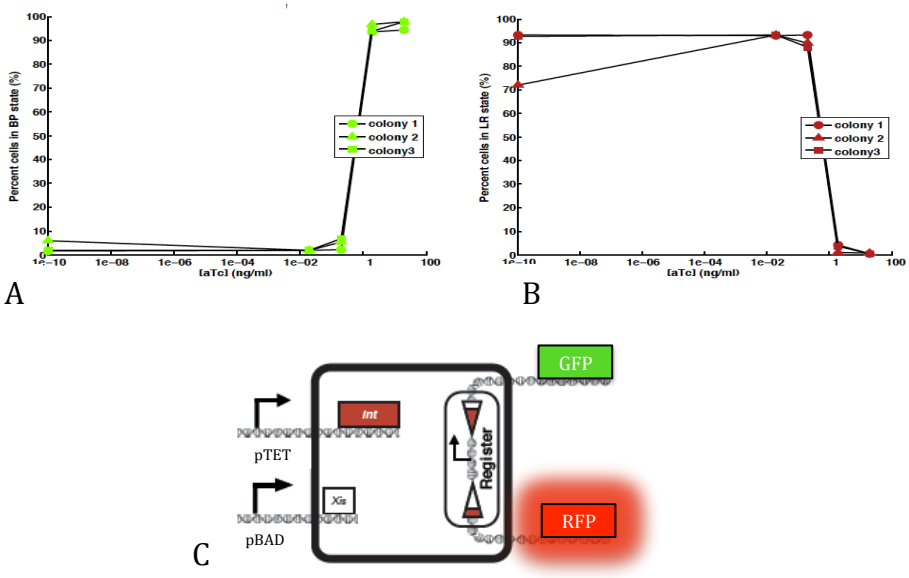

Fig. 22 (A and B) Input-state dose response of aTc induced integrase from H3 D-latch in DH5αZ1H3 measured with the flow cytometer. Excisionase was expressed under the control of an ara inducible promoter, induced with a fixed ara concentration (0.5% ara weight/volume concentration in the media). Integrase was expressed under the control of a tetracycline promoter. We showed the fraction of BP state (A) and LR state (B) under different aTc concentrations (0ng/ml, 0.2ng/ml, 2ng/ml, 20ng/ml and 200ng/ml). The three clones used in (A) and (B) were the same. The x-axes show the act concentration in ng/ml on a log scale. The y-axes show the percentage of cells in BP (green) or LR (red) state. (C) shows the RAD module in the initial condition.

3.2.2 Construction of measurement vector

Using this measurement vector, we wanted to be able to determine the relative input strengths (in RPU) of the promoters driving integrase/excisionase expression that were required to reach a stoichiometry between the two proteins, which allowed complete LR to BP recombination. We were using standardized promoters and RBSs, which provided several advantages: (i) The relative promoter units for these promoters were well described and (ii) the RBSs strengths were not sensitive to the 5'UTR sequence of the gene being expressed. Therefore the relative ranking between the promoters/RBSs pairs remained the same independently from the downstream gene, allowing reliable comparison between the different integrase and excisionase concentrations and facilitating the incorporation of the experimental data into a mathematical model.

The measurement vector design consisted of antiparallel orientated integrase and excisionase cassettes flanked by a standardized bicistron. Between the two bicistrons our design included two BsaI cut sites to allow cloning of different promoters, controlling transcription of integrase and excisionase. As a backbone plasmid we used SR5A that contained of a low copy of origin of replication and a biobrick pre- and suffix. In our first design, the integrase assembly fragment consisted of an antiparallel integrase gene with the sequence of a his-tag that had at the 3'end an overlap with the backbone gene. The excisionase assembly fragment consisted of an excisionase gene with the sequence of a his-tag and had at the 5' end an overlap with the backbone gene. The GBU1 consisted of an antiparallel bicistron RBS, a BsaI cut side at the 5'end and an overlap with integrase gene at the 3'end. GBU2 consisted of a bicistron RBS, a BsaI cut side at the 3'end and an overlap with excisionase gene at the 5'end.

As the first design could not be assembled together, we generated a second design that we were not able to assemble in the given time frame. In the second design, the integrase and excisionase assembly fragments consisted of an antiparallel integrase gene and an excisionase gene. The backbone had at the 3'end an overlap with the integrase gene and at the 5'ends an overlap with the excisionase gene. GBU1 and GBU2 consisted of the same parts like in the first design.

In the following, we will show what we accomplished to construct the measurement vector from its initial design.

Because of the various problems we tried to accomplish the construction of the initial design with different assembly methods. Neither with Gibson assembly nor with CPEC we were able to assembly the whole vector. We tried to assemble part by part in relying reactions. Neither with Gibson assembly nor with Assembly PCR we were able to assemble more than three pieces together (Fig. 23 C, line 1 for Gibson assembly). None of the transformed bacteria showed the inserted construct after colony PCR.

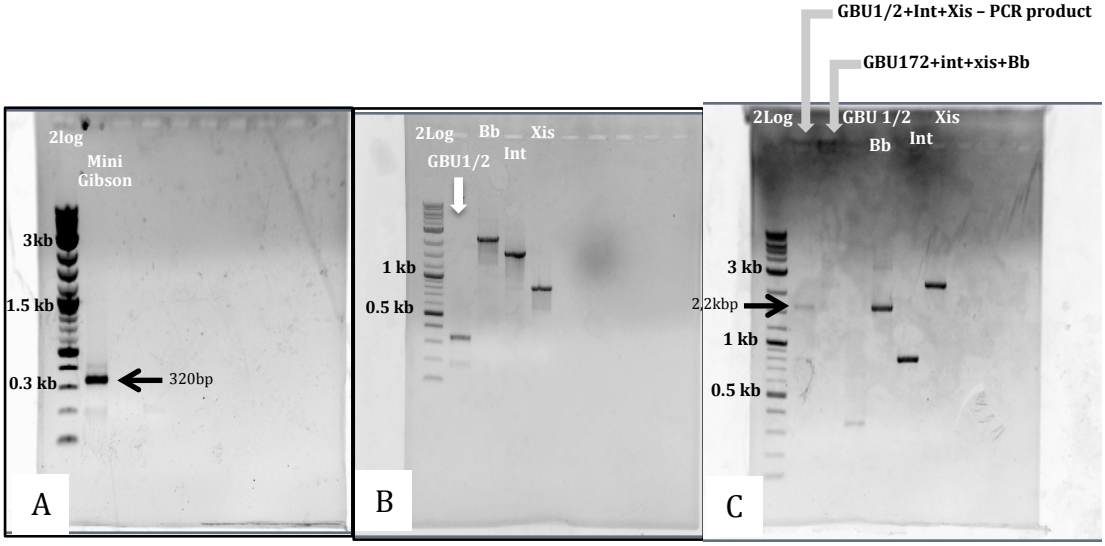

Fig. 23 (A) shows the PCR product of a Gibson assembly of GBU1 and GBU2. We can see a band of the expected length. (B) shows the PCR product of all three fragments for Gibson assembly: GBU1/2 (300bp), Bb (2,4kbp), int (1,5kbp) and xis (0,7kbp). We can see all bands at the expected lengths. (C) shows in the first line the assembly product of a Gibson assembly of int+GBU1/2+xis (around 2.2kbp), line two shows unsuccessful assembly of GBU1/2+int+xis+Bb (expected length: 6kbp). Line 3 to 5 show fragments for comparison.

4 Discussion

4.1 In silico experiments

4.1.1 A simplified computational teaching model of the RAD

We generated a teaching model that fulfilled the aim of giving a basic understanding of the RAD system and modeling of recombination systems. The teaching model could simulate the three operations (set, reset and hold) of the RAD module, depending on the initial starting conditions provided by the user. The model was capable of capturing the following experimental observed behaviors of the RAD. First the teaching model could recapitulate a state switching and data storage function provided by the integrase-excisionase system. Second and like the full model in the Bonnet et al. paper, the teaching model could predict the boundaries between the set and the reset regime, determined by the excisionase level but not so much by the integrase level. This second phenomenon was expected because we assumed that excisionase only interacts with DNA bound integrase (Ghosh, Bibb et al. 2008; Bonnet, Subsoontorn et al. 2012). Nonetheless, and as we expected, the following behaviors could not be captured: First, at a low amounts of DNA data register, the system did not show a hold state. This behavior resulted from the assumption that integrase and excisionase functioned as monomers. Without the cooperativity arising from the multimerisation enzyme process, we did not have a switch like behavior in the presence of low-level integrase expression. In fact, various studies have shown that cooperativity is an important factor in natural systems exhibiting switch like behavior (Ferrell 2002). The teaching model is now available and can be used to teach basic understanding of modeling. The presented teaching model can be also used as a building block or as starting point for more sophisticated modeling projects.

4.1.2 A quantitative computational model of the RAD module behavior using realistic reaction rates

Based on the teaching model we generated the first quantitative model with realistic reaction rates of the RAD module. For the realistic reaction rates of the RAD model that we designed we used the assumptions of the published model (Bonnet, Subsoontorn et al. 2012). Unlike the teaching model, we could simulate with the realistic reaction rates of the RAD model all operation rates, not limited by any starting conditions. Unlike the published model, the realistic reaction rate model presented here can be reconfigured more easily upon new knowledge about biochemical reactions. The simulated data of the realistic reaction rates of the RAD model allowed for the first time to map the boundaries between states the input strength of the RAD module in real physical units. We have shown that the simulated results of the model were not in conflict with the experimental results of the Bonnet et al. paper in terms of switching time and operational lifetime. We used the model to predict the boundaries, with respect to the integrase and excisionase production rates (in nM/min), between the different operation regions (set, reset and hold). At 1000min (about 16hrs) of reaction time, the boundary between set and reset was predicted to be at 6.813nM/min of excisionase production, which corresponded to approximately 6molecules/cell/min. For the boundary between set and hold we predicted 0.5623nM/min which corresponded to approximately 0.5molecules/cell/min of integrase production, therefore the predicted functional excisionase/integrase ratio, all other things being equal, was approximately 12, close to the in vitro measurements that can be found in literature (Ghosh, Wasil et al. 2006). We also explored how predicted operable region boundaries were sensitive to our choice of parameters. For all explored parameters, we discovered that increasing the parameter values had nearly no effect on the state boundaries of the RAD. When we decreased the parameters, the RAD lost the reset region at least in the time frame of the simulation. With more experimental results, we would be able to refine the model for better and more precise predictions of the boundaries between the three states. Future work could be to improve the assumptions that we made and add more relevant parameters. The model and all its future improvements would be beneficial to the design of a new RAD system as well as for using the RAD in higher order compositions.

4.2 In vivo experiments

4.2.1 A new bacterial chassis for quantitative measurements of the RAD module behavior

We have engineered the RAD module into a new chassis, BW27786 that is capable of responding to arabinose induction linearly. We engineered strains derived from BW27786 with a chromosomally integrated DNA data register in LR or BP orientation and with Kanamycin or Chloramphenicol antibiotic resistance cassette.
This was the first time that the unchanged RAD module, which was optimized for a specific *E.coli* strain (DH5αZ1), was moved to a new genetic environment. The observed changes gave information about the portability of the RAD.
In future, the tetracycline repressor cassette has to be cloned into a new chassis so that all set, reset, and hold operations can be performed using the existing set and reset generators (controlled by pTET and pBAD). Linear response to arabinose induction enables researchers to fine-tune the production of integrase and excisionase independently to better understand the operational behavior of the RAD module. Data obtained using this new chassis can be used to improve the quantitative computational model of the RAD.

4.2.2 Standard curves for arabinose and tetracycline inducible promoters activities

In this study we reproduced and improved the resolution of the measurements of the Khlebnikov et al. paper that showed linear induction of arabinose inducible promoter activity in BW27786. We expanded the study for characterization of the induction behavior of arabinose inducible promoter in DH5αZ1. We mapped the arabinose concentration to the promoter activity in percent based on the expression rates of the reporter gene GFP.
We assumed that the arabinose inducible promoter activity reached at 0.2% arabinose concentration a steady state. Although this was not shown in our experiments, it correlated with already published results (Lutz and Bujard, 1997; Klebnikov, 2001). This standard curve was used in this study and will be available for future studies to map the arabinose concentration to promoter activities.
We characterized the response of the tetracycline inducible promoter for DH5αZ1. Our measurement resolution was not sufficient for claiming the linear induction of the promoter activity. However, our observed low-resolution response curve matched higher resolution study results from Lutz and Bujard et al paper that showed the linear induction of the promoter activity. The results should be the same for BW27786, because there is no mutation reported that is known to cause a different behavior of BW27786. We were not able to perform the described experiments with BW27786 because the strain did not include a tetracycline repressor. A tetracycline inducible promoter (pTET) is constitutively active in BW27786. Note, that we used the fluorescence of GFP to correlate the promoter activity to the inducer concentration. Further work is needed to provide a better understanding of the promoter activity. Especially for the tetracycline induced promoter, measurements with higher resolution are needed to give a clearer understanding of the behavior of the inducible promoter.

4.2.3 Characterization of the transition regimes of the RAD between hold-set, set-reset and reset-hold.

4.2.3.1 Hold/Set Boundary

In our first study we used an ara inducible set switch to explore the boundaries between set and hold state in BW27786 and DH5αZ1. We found that thresholds for complete switching appeared between an arabinose concentration of $4*10^{-5}$% and $8*10^{-5}$% for BW27786. For DH5αZ1, we showed that an arabinose concentration above $8*10^{-8}$% was necessary to switch the system reliably to LR across three different clones. Thus we claimed this concentration as the threshold point. When we compared the measurements with our standard curve, we saw that for both strains a promoter activity around 10% produced sufficient amounts of integrase to switch the RAD.

4.2.3.2 Set/Reset Boundary

To explore the boundary between set and reset, we used another construct, a D-Latch H3 in DH5αZ1 and in BW27786. In D-Latch H3 the integrase was under the control of a pTET promot-

er and excisionase under the control of a pBAD promoter. To explore the boundary we fixed the activity of the pTET promoter for integrase, with fixed amounts of aTc for DH5αZ1 or because of the absence of the tet repressor in BW27786. The measurement points showed that the threshold for reset in BW27786 and for DH5αZ1 was bellow $5*10^{-4}$% arabinose concentration.

4.2.3.3 Hold/Reset Boundary

Next we explored the boundaries between reset and hold in DH5αZ1. We used the same D-latch as for the studies of the boundary between set and reset. In this study we kept the arabinose concentration constantly and varied the concentration of aTc. We observed a switch like behavior above 2ng/ml concentration of aTc for the DNA data register. Future studies should explore the boundary region with a higher resolution. Like in the previous studies it will be needed to correlate the promoter activity to relative promoter units. In this study we have not explored the reset hold transition region for BW27786. Because the strain has not been engineered to have the tet repressor cassette.

For a complete characterization of the RAD, further work is needed on all presented experiments. The standard curve for promoter activity for arabinose and tetracycline inducible promoters should be further refined and linked to RPU. This could improve the results for all future studies. Also more data points, especially for the reset set and reset hold transition, are needed to be able to make more precise conclusions. Also in the BW27786 strain the tetracycline repressor has to be chromosomally integrated. Then it would be possible to make the tetracycline inducible reset-hold transition experiment and the arabinose inducible set-reset experiments in a way that the results are completely comparable with the results obtained in the DH5αZ1 chassis. However, this system presented several intrinsic limitations that prevented its use for an advanced, fully quantitative characterization of the RAD module behavior: (i) the reporter system that we used for the standard curve was not sensitive enough (ii) the standard curve was made for a different protein than integrase and excisionase (iii) the standard curve was not linked to a standard unit like RPU. Nevertheless and despite these limitations, we obtained useful results that increased our understanding of the RAD system.

4.2.4 Construction of the measurement vector

Because of the explained drawbacks of the inducible measurement system we wanted to use another measurement system. Unfortunately, we have not successfully constructed a measurement vector yet in this project. The construction problems could have occurred because of multiple reasons. The measurement vector included four hairpin structures that could have caused problems for assembling. Also the two antiparallel bicistrons were able to from a strong hairpin structure. The initial design of the overlapping regions between DNA pieces to be assembled was not optimal. Some of the overlapping regions included hairpin structures and we found other regions on the plasmid that matched to the overlaps. In the second design of our parts for Gibson Assembly, we avoided hairpin structures, but it still did not work. Therefore it would have been possible and easier to synthesize the whole measurement plasmid.

5 Conclusion

During this project we focused on refining the rewritable addressable recombinase data storage module (RAD) to a standard device. This device could be used in future designs and applications. Quantitative characterization is the first step of standardization. The project consisted of in silico and in vivo studies to get a better understanding of the RAD module. We generated a computational teaching model to give students a basic understanding of the RAD module and of modeling principles of DNA recombination systems. The teaching model is a simplified version of the available model of the RAD module (Bonnet, Subsoontorn et al. 2012) and could simulate all three transition states (set, reset and hold) under given certain proper starting conditions. Based on the teaching model we generated the first quantitative model capable of simulating the behavior of the DNA data register with realistic reaction rates. We could visualize the simulated data as heat maps that showed the boundaries between the different states. The simulated results of the model were in accord with the experimental results of the Bonnet et al. paper in terms of switching time and the operational lifetime. As an improvement to the initial published model, the rRAD supported easy inclusion of new, experimentally obtained knowledge of the biochemical reactions, occurring in the system. To verify our model we designed experiments to explore the boundaries between the different states. We measured the switching thresholds for the three transition states with inducible generators. The experimental results showed the same trend like the modeling results. For our experiments we built a new chassis and transferred the RAD module to this chassis. The functionality of the RAD module in the new chassis proved its portability.

Further work is needed to include more and sophisticated experimental data to generate higher resolution heat maps of the results. These data can then be compared to the simulation results and can also be fed in the model, to generate a better version. In addition useful biochemical and biophysical knowledge can be included into the model. Future work has to be done to get a complete characterization of the RAD to use it as a standard device.

In conclusion, the presented work is a first step to give a better understanding of the RAD module. This knowledge is needed to apply higher device composition and for applicable designs.

Literature

Andersen, J. B., C. Sternberg, et al. (1998). "New unstable variants of green fluorescent protein for studies of transient gene expression in bacteria." Applied and environmental microbiology **64**(6): 2240-2246.

Arkin, A., J. Ross, et al. (1998). "Stochastic kinetic analysis of developmental pathway bifurcation in phage lambda-infected Escherichia coli cells." Genetics **149**(4): 1633-1648.

Bonnet, J., P. Subsoontorn, et al. (2012). "Rewritable digital data storage in live cells via engineered control of recombination directionality." Proceedings of the National Academy of Sciences of the United States of America **109**(23): 8884-8889.

Buchler, N. E., U. Gerland, et al. (2005). "Nonlinear protein degradation and the function of genetic circuits." Proceedings of the National Academy of Sciences of the United States of America **102**(27): 9559-9564.

Burrill, D. R. and P. A. Silver (2010). "Making cellular memories." Cell **140**(1): 13-18.

Ferrell, J. E., Jr. (2002). "Self-perpetuating states in signal transduction: positive feedback, double-negative feedback and bistability." Current opinion in cell biology **14**(2): 140-148.

Gardner, T. S., C. R. Cantor, et al. (2000). "Construction of a genetic toggle switch in Escherichia coli." Nature **403**(6767): 339-342.

Ghosh, P., L. A. Bibb, et al. (2008). "Two-step site selection for serine-integrase-mediated excision: DNA-directed integrase conformation and central dinucleotide proofreading." Proceedings of the National Academy of Sciences of the United States of America **105**(9): 3238-3243.

Ghosh, P., A. I. Kim, et al. (2003). "The orientation of mycobacteriophage Bxb1 integration is solely dependent on the central dinucleotide of attP and attB." Molecular cell **12**(5): 1101-1111.

Ghosh, P., N. R. Pannunzio, et al. (2005). "Synapsis in phage Bxb1 integration: selection mechanism for the correct pair of recombination sites." Journal of molecular biology **349**(2): 331-348.

Ghosh, P., L. R. Wasil, et al. (2006). "Control of phage Bxb1 excision by a novel recombination directionality factor." PLoS biology **4**(6): e186.

Gibson, D. G. (2011). "Enzymatic assembly of overlapping DNA fragments." Methods in enzymology **498**: 349-361.

Haldimann, A. and B. L. Wanner (2001). "Conditional-replication, integration, excision, and retrieval plasmid-host systems for gene structure-function studies of bacteria." Journal of bacteriology **183**(21): 6384-6393.

Ham, T. S., S. K. Lee, et al. (2008). "Design and construction of a double inversion recombination switch for heritable sequential genetic memory." PloS one **3**(7): e2815.

Hanahan, D. (1983). "Studies on transformation of Escherichia coli with plasmids." Journal of molecular biology **166**(4): 557-580.

Khlebnikov, A., K. A. Datsenko, et al. (2001). "Homogeneous expression of the P(BAD) promoter in Escherichia coli by constitutive expression of the low-affinity high-capacity AraE transporter." Microbiology **147**(Pt 12): 3241-3247.

Kramer, B. P., A. U. Viretta, et al. (2004). "An engineered epigenetic transgene switch in mammalian cells." Nature biotechnology **22**(7): 867-870.

Lutz, R. and H. Bujard (1997). "Independent and tight regulation of transcriptional units in Escherichia coli via the LacR/O, the TetR/O and AraC/I1-I2 regulatory elements." Nucleic acids research **25**(6): 1203-1210.

McGinness, K. E., T. A. Baker, et al. (2006). "Engineering controllable protein degradation." Molecular cell **22**(5): 701-707.

Podhajska, A. J., N. Hasan, et al. (1985). "Control of cloned gene expression by promoter inversion in vivo: construction of the heat-pulse-activated att-nutL-p-att-N module." Gene **40**(1): 163-168.

Quan, J. and J. Tian (2009). "Circular polymerase extension cloning of complex gene libraries and pathways." PloS one **4**(7): e6441.

Ringrose, L., V. Lounnas, et al. (1998). "Comparative kinetic analysis of FLP and cre recombinases: mathematical models for DNA binding and recombination." Journal of molecular biology **284**(2): 363-384.

Ro, D. K., E. M. Paradise, et al. (2006). "Production of the antimalarial drug precursor artemisinic acid in engineered yeast." Nature **440**(7086): 940-943.

Appendix

MatLab code for teaching model

```
y(1)=BP; y(2)=BPI; y(3)=BPIE; y(4)=I; y(5)=LRI; y(6)=LR; y(7)=E; y(8)=LRIE
r1=1; r2=1; r3=1; r4=1; r5=1; r6=1; r7=1; r8=1; r9=1; r10=1;
dy(1) = r2*y(2)-r1*y(1)*y(4); - reaction of BP
dy(2) = r1*y(1)*y(4)+r6*y(3)-r2*y(2)-r5*y(2)*y(7)-r3*y(2); - reaction of BPI
dy(3) = r5*y(2)*y(7)+r9*y(8)-r6*y(3); - reaction of BPIE
dy(4) = r2*y(2)+r4*y(5)-r1*y(1)*y(4)-r10*y(6)*y(4); - reaction of I
dy(5) = r3*y(2)+r8*y(8)+r10*y(6)*y(4)-r4*y(5)-r7*y(5)*y(7); - reaction of LRI
dy(6) = r4*y(5)-r10*y(6)*y(4); - reaction of LR
dy(7) = r6*y(3)+r8*y(8)-r7*y(5)*y(7)-r5*y(2)*y(7); - reaction of E
dy(8) = r7*y(5)*y(7)-r8*y(8)-r9*y(8); - reaction of LRIE
```

We could solve and plot this using the following MATLAB code:

```
function LRfrac=DLatch1(int,xis,BP,LR,T)
% The function DLatch1 take five inputs: int = initial amount of integrase, xis = initial amount of integrase, BP = initial amount of DNA data register in BP state, LR = initial amount of DNA data register in LR state, T = time in arbitrary units. The function returns the output, LRfrac, which is the fraction of the DNA data register in the LR state.
[T,Y] = ode23s(@rigid,[0 T],[BP 0 0 int 0 LR xis 0]);
% We used the MATLAB function ode23s to solve ode definite by a function “rigid”. T is a time point output and Y is the amount of different species at different time points. The code keep track of eight species.
1: BP  - this is the DNA data register in the BP state. The initial amount is defend by the input of the function D-Latch
2: BPI – this is the DNA data register in the BP state that is bound to integrase. The initial amount is zero.
3: BPIE – this is the DNA data register in the BP state bound to integrase and excisionase. The initial amount is zero.
 4: I – this is integrase. The initial amount is defined by the input of the function DLatch1
 5: LRI – this is the DNA data register in the LR state bound to integrase. The initial amount is zero.
6: LR – this is the DNA data register in the LR state. The initial amount is defended by the input of the function DLatch1
7: E – this is excisionase. The initial amount is defined by the input of the function DLatch1
8: LRIE - this is the DNA data register in the LR state bound to integrase and excisionase. The initial amount is zero.


figure(1),
% Figure 1 show the time course kinetics of the tatal BP (in blue) and total LR (in black)
plot(T,Y(:,1)+Y(:,2)+Y(:,3)), hold on %this is total of BP
plot(T,Y(:,5)+Y(:,6)+Y(:,8),'color','k') %this is total of LR

BPtotalfinal=Y(end,1)+ Y(end,2)+ Y(end,3);
% The total amount of BP at the final timepoint in the simulation (is equal to BP+BPI+BPIE)
LRtotalfinal=Y(end,5)+ Y(end,6)+ Y(end,8);
% The total amount of LR at the final timepoint in the simulation (is equal to LR+LRI+LRIE)
LRfrac= LRtotalfinal/(BPtotalfinal+LRtotalfinal);% final Output
function dy = rigid(t,y)
dy = zeros(8,1);    % a column vector
r1=1; r2=1; r3=1; r4=1; r5=1; r6=1; r7=1; r8=1; r9=1; r10=1;
% r1-r10 are the reaction rate constance that we assume are equal to 1.
dy(1) = r2*y(2)-r1*y(1)*y(4); %reaktion of BP
```

```
dy(2) = r1*y(1)*y(4)+r6*y(3)-r2*y(2)-r5*y(2)*y(7)-r3*y(2); %reaktion of BPI
dy(3) = r5*y(2)*y(7)+r9*y(8)-r6*y(3); %reaktion of BPIE
dy(4) = r2*y(2)+r4*y(5)-r1*y(1)*y(4)-r10*y(6)*y(4); %reaktion of I
dy(5) = r3*y(2)+r8*y(8)+r10*y(6)*y(4)-r4*y(5)-r7*y(5)*y(7); %reaktion of LRI
dy(6) = r4*y(5)-r10*y(6)*y(4); %reaktion of LR
dy(7) = r6*y(3)+r8*y(8)-r7*y(5)*y(7)-r5*y(2)*y(7); %reaktion of E
dy(8) = r7*y(5)*y(7)-r8*y(8)-r9*y(8); %reaktion of LRIE
```

Mat Lab code for Realistic reaction rate model

```
function LRfrac=DLatchNight(int,xis,BP,LR,T)
initcon=zeros(35,1);
% specifying initial condition.
initcon(1)= BP;
initcon(6)= LR;
initcon(34)=int;
initcon(35)=xis;

[T,Y] = ode23s(@DlatchODEs,T ,initcon);

%% generate plot from within the function (
%figure(1),
%
plot(T,Y(:,1)+Y(:,2)+Y(:,3)+Y(:,4)+Y(:,5)+Y(:,21)+Y(:,22)+Y(:,23)+Y(:,24)+Y
(:,25)+Y(:,26)+Y(:,27)+Y(:,28)+Y(:,29)+Y(:,30)), hold on %this is total of
BP
%subplot(2,1,1)
%plot(T,Y(:,2)+2*Y(:,3)+3*Y(:,4)+4*Y(:,5)+Y(:,7)+2*Y(:,8)+3*Y(:,9)+4*Y(:,10
)+Y(:,11)+Y(:,12)+Y(:,13)+3*Y(:,14)+Y(:,15)+Y(:,16)+Y(:,17)+Y(:,18)+Y(:,19)
+Y(:,20)+Y(:,21)+Y(:,22)+Y(:,23)+Y(:,24)+Y(:,26)+Y(:,27)+Y(:,28)+Y(:,29)+Y(
:,30)+Y(:,31)+2*Y(:,32),'color','g'), hold on %this is total of I
%subplot(2,1,2)
%plot(T,Y(:,6)+Y(:,7)+Y(:,8)+Y(:,9)+Y(:,10)+Y(:,11)+Y(:,12)+Y(:,13)+Y(:,14)
+Y(:,15)+Y(:,16)+Y(:,17)+Y(:,19)+Y(:,20),'color','k') %this is total of LR
%
plot(T,Y(:,11)+Y(:,12)+2*Y(:,13)+Y(:,14)+2*Y(:,15)+Y(:,16)+2*Y(:,17)+3*Y(:,
18)+3*Y(:,19)+4*Y(:,20)+4*Y(:,21)+3*Y(:,22)+2*Y(:,23)+3*Y(:,24)+2*Y(:,25)+Y
(:,26)+Y(:,27)+Y(:,28)+2*Y(:,29)+Y(:,30)+Y(:,33),'color','m') %this is
taltal of E
% Y(end,:);
% figure(2),
% plot(T,Y(:,31)),hold on
% plot(T,Y(:,34),'color','k')
% plot(T,Y(:,3),'color','g')
% plot(T,Y(:,5),'color','y')
% plot(T,Y(:,27),'color','r')

%%
BPtotal = sum(Y(:, 1:5), 2)+ sum(Y(:, 21:30), 2);
LRtotal = sum(Y(:, 6:20), 2);
LRfrac= LRtotal./(BPtotal+LRtotal);%final Output

%BPtotalfinal=Y(end,1)+ Y(end,2)+ Y(end,3);
%LRtotalfinal=Y(end,5)+ Y(end,6)+ Y(end,8);
%LRfrac= LRtotalfinal/(BPtotalfinal+LRtotalfinal);%final Output
function dy = DlatchODEs(t,y)
BP=y(1);
BPI=y(2);
BPI2=y(3);
BPI2I=y(4);
BPI2I2=y(5);
```

```
LR=y(6);
LRI=y(7);
LRI2=y(8);
LRI2I=y(9);
LRI2I2=y(10);
LRIE=y(11);
LRI2E=y(12);
LRI2E2=y(13);
LRI2IE=y(14);
LRI2IE2=y(15);
LRI2I2E=y(16);
LRI2I2E2=y(17);
LRI2IE2E=y(18);
LRI2I2E2E=y(19);
LRI2I2E2E2=y(20);

BPI2I2E2E2=y(21);
BPI2I2E2E=y(22);
BPI2I2E2=y(23);
BPI2IE2E=y(24);
BPI2IE2=y(25);
BPI2IE=y(26);
BPI2I2E=y(27);
BPI2E=y(28);
BPI2E2=y(29);
BPIE=y(30);

I=y(31);
I2=y(32);
E=y(33);
int=y(34);
xis=y(35);

 %diffusion limited binding rate 1e8 /M/s = 0.1/nM/s = 6/nM/min
 % to make this simple I would just keep at ~ 1 nM/min (same order of mag)
diffLim = 1; %nM/min
% Dissociation equilbrium constant of integrase dimer (Ki) is unknown; we
just
% gonna use 'a typical' 10 nM Kd as used in Buchler et al 2005 PNAS paper
% table-1. the dissociatio rate, k10 is Ki*diffLim
Ki = 1; % nM
% From Ghosh et al 2005 JMB paper figure-1, dissociation equilibrium
constant for
% integrase dimer - attB or attP site are 70 nM and integrase dimer - attL
% or att R are 15 nM. We just gonna estimate this dissociation equilibrium
% between flippee and integrase dimer (Kdi) at 30 nM. Thus, all the binding
% dissociation rate constant between flipee and integraes dimer (k12, k14,
% k16, k22, )are % approximately diffLim*Kdi
Kdi = 30; % nM
% Intgrase-excisionase dissociation equilibrium constant is unknown. We
% will just use the same number as a `typical' dimerization equilibrium
% constant for protein dimer as we use above (since both cases are
% protein-protein interaction). The dissociation rate constant is thus
% approximately diffLim*Kdix
Kdix = 100; % nM
% Catalytic rate of BP to LR and LR to BP recombinations are unknown. The
% only recombination catalytic rate we have seen are from Ringrose et al
% 1998 JMB paper table-3 which shows the catalytic rate of Cre and Flp to
% be 0.006 /sec and 0.04 /sec, respectively. (~0.36 /min and 2.4 /min,
respectively).
% We will use these as a 'typical' recombination catalytic (kc) rate of
% 1/min.
kc = 10; %/min
% Promoter clearance rate is at the maximal ~ 1 per sec (60 bases per
% second RNAP speed). The number of protein produced per RNA transcript is
% about 10 per mRNA (took this number from Arkin et al 1998 Genetics paper
```

```
% table-2). Thus, we can give protein output per gene up to say, 600
molecules
% (nM)per minute. However, in our case, we usually use very weak RBS and
% sometimes gtg start codon and sub optimal promoter. Thus, our protein
output range
% could be much lower.Let's start with 1 nM/gene/min. In our plot we scale
% integrase and excisionase production by scaling 'int' and 'xis' parameter
% value which, in our case, will give the same result as scaling intProd
% and xisProd. In other words, x- and y- axis on the heatmap indicate xis
% and int production in nM/min unit
intProd = 1; %/min
xisProd = 1; %/min
% protein degradation and dilution rate depend on protein stability and
% rate of cell growth, respectively. At the minimal, protein level comes
% down by cell growth and division. We use a typical E.coli cell cycle of
% 20 min to by a half-life of protein due to dilution so the degradation &
% dilution is at least log(2)/20 /min ~ 0.03/min. With active degradation
% protein half life can go down to a minute (need to check ref, vaguely
% remember from Sauer's lab lambda-ssrA degradation study) to the
% degradation + dilution rate can be as high has log(2)/1 ~ 1 /min. Here we
% just go with an intermediate range of ~ 0.1 min
ky = 1; %/min


dy = zeros(35,1);
k1=0; % BP      + I -> BPI
k2=0; % BP      + I <- BPI
k3=0; % BPI     + I -> BP(I2)
k4=0; % BPI     + I <- BP(I2)
k5=0; % BP(I2)  + I -> BP(I2)I
k6=0; % BP(I2)  + I <- BP(I2)I
k7=0; % BP(I2)I + I -> BP(I4)
k8=0; % BP(I2)I + I <- BP(I4)
k9=diffLim; % I + I       -> I2
k10=Ki*diffLim;% I + I       <- I2

k11=diffLim; % BP     + I2 -> BP(I2)
k12=Kdi*diffLim; % BP     + I2 <- BP(I2)
k13=diffLim; % BP(I2) + I2 -> BP(I4)
k14=Kdi*diffLim; % BP(I2) + I2 <- BP(I4)
k15=kc; % BP(I4)      -> LR(I4)
k16=Kdi*diffLim; % LR(I4)      -> LR(I2)  + I2
k17=diffLim; % LR(I4)      <- LR(I2)  + I2
k18=0; % LR(I4)      -> LR(I2)I + I
k19=0; % LR(I4)      <- LR(I2)I + I
k20=0; %LR(I2)I      -> LR(I2) + I

k21=0; %LR(I2)I <- LR(I2) + I
k22=Kdi*diffLim; %LR(I2)  -> LR + I2
k23=diffLim; %LR(I2)  <- LR + I2
k24=0; %LR(I2)  -> LRI + I
k25=0; %LR(I2)  <- LRI + I
k26=0; %LRI    -> LR + I
k27=0; %LRI    <- LR + I
k28=0;
k29=0;
k30=diffLim; %LR(I2) + E  -> LR(I2)E

k31=Kdix*diffLim; %LR(I2) + E   <- LR(I2)E
k32=diffLim; %LR(I2)E + E  -> LR(I2)(E2)
k33=Kdix*diffLim; %LR(I2)E + E  <- LR(I2)(E2)
k34=0;
k35=0;
k36=0;
k37=0;
k38=0; %LR(I2)I(E2)  + E  -> LR(I2)I(E2)E
```

```
k70=0; %LR(I2)I(E2)  + E  <- LR(I2)I(E2)E

k39=diffLim; %LR(I4)       + E  -> LR(I4)E
k40=Kdix*diffLim; %LR(I2)       + E  <- LR(I2)E

k41=diffLim; %LR(I4)E         + E  -> LR(I4)(E2)
k42=Kdix*diffLim; %LR(I4)E         + E  <- LR(I4)(E2)
k43=diffLim; %LR(I4)(E2)      + E  -> LR(I4)(E2)E
k44=Kdix*diffLim; %LR(I4)(E2)      + E  <- LR(I4)(E2)E
k45=diffLim; %LR(I4)(E2)E     + E  -> LR(I4)(E4)
k46=Kdix*diffLim; %LR(I4)(E2)E     + E  <- LR(I4)(E4)
k47=kc; %LR(I4)(E4)        -> BP(I4)(E4)
k48=Kdix*diffLim; %BP(I4)(E4)           -> BP(I4)(E2)E + E
k49=diffLim; %BP(I4)(E4)           <- BP(I4)(E2)E + E
k50=Kdix*diffLim; %BP(I4)(E2)E          -> BP(I4)(E2)  + E

k51=diffLim; %BP(I4)(E2)E          <- BP(I4)(E2)  + E
k52=Kdix*diffLim; %BP(I4)(E2)           -> BP(I4)E     + E
k53=diffLim; %BP(I4)(E2)           <- BP(I4)E     + E
k54=Kdix*diffLim; % BP(I4)E       -> BP(I4) + E
k55=diffLim; % BP(I4)E       <- BP(I4) + E
k56=0;
k57=0;
k58=0;
k59=0;
k60=0;

k61=0;
k62=Kdix*diffLim; % BP(I2)(E2)       -> BP(I2)E + E
k63=diffLim; % BP(I2)(E2)       <- BP(I2)E + E
k64=Kdix*diffLim; % BP(I2)E          -> BP(I2)  + E
k65=diffLim; % BP(I2)E          <- BP(I2)  + E
k66=0;
k67=0;
k68=intProd; % int -> int + I
k69=xisProd; % xis -> xis + E

k71=ky; % I  -> or I2 -> I
k72=ky; % E  ->


dy(1) = k2*BPI + k12*BPI2 - k1*BP*I - k11*BP*I2; %*** dBP/dt
%%dy(2) = k1*BP*I+k4*BPI2+k66*BPIE-k2*BPI-k3*BPI*I-k67*BPI*E; %*** dBPI/dt

dy(3) = k3*BPI*I - k4*BPI2 - k5*BPI2*I + k6*BPI2I ...
        + k11*BP*I2 - k12*BPI2-k13*BPI2*I2 +k14*BPI2I2 ...
        + k64*BPI2E -k65*BPI2*E;   %*** dBP(I2)/dt

%%dy(4) = k5*BPI2*I+k8*BPI2I2+k60*BPI2IE-k6*BPI2I-k7*BPI2I*I-
k61*BPI2I*E;*** dBP(I2)I/dt

dy(5) = k7*BPI2I*I - k8*BPI2I2 + k13*BPI2*I2 - k14*BPI2I2 ...
        -k15*BPI2I2 ...
        +k54*BPI2I2E - k55*BPI2I2*E; %*** dBP(I4)/dt

dy(6) = +k22*LRI2 - k23*LR*I2 + k26*LRI - k27*LR*I; %*** dLR/dt
%%dy(7) = k24*LRI2+k27*LR*I+k29*LRIE-k25*LRI*I-k26*LRI-k28*LRI*E;
%*** dLRI/dt

dy(8) =   k16*LRI2I2 -k17*LRI2*I2 + k20*LRI2I - k21*LRI2*I ...
         -k22*LRI2 + k23*LR*I2  - k24*LRI2 + k25*LRI*I ...
         -k30*LRI2*E + k31*LRI2E; % dLR(I2)/dt

%%dy(9) = k18*LRI2I2+k21*LRI2*I+k35*LRI2IE-k19*LRI2I*I-k20*LRI2I-k34* func-
```

```
tion LRfrac=DLatchNight(int,xis,BP,LR,T)
initcon=zeros(35,1);
% specifying initial condition.
initcon(1)= BP;
initcon(6)= LR;
initcon(34)=int;
initcon(35)=xis;

[T,Y] = ode23s(@DlatchODEs,T ,initcon);

%% generate plot from within the function (
%figure(1),
%
plot(T,Y(:,1)+Y(:,2)+Y(:,3)+Y(:,4)+Y(:,5)+Y(:,21)+Y(:,22)+Y(:,23)+Y(:,24)+Y
(:,25)+Y(:,26)+Y(:,27)+Y(:,28)+Y(:,29)+Y(:,30)), hold on %this is total of
BP
%subplot(2,1,1)
%plot(T,Y(:,2)+2*Y(:,3)+3*Y(:,4)+4*Y(:,5)+Y(:,7)+2*Y(:,8)+3*Y(:,9)+4*Y(:,10
)+Y(:,11)+Y(:,12)+Y(:,13)+3*Y(:,14)+Y(:,15)+Y(:,16)+Y(:,17)+Y(:,18)+Y(:,19)
+Y(:,20)+Y(:,21)+Y(:,22)+Y(:,23)+Y(:,24)+Y(:,26)+Y(:,27)+Y(:,28)+Y(:,29)+Y(
:,30)+Y(:,31)+2*Y(:,32),'color','g'), hold on %this is total of I
%subplot(2,1,2)
%plot(T,Y(:,6)+Y(:,7)+Y(:,8)+Y(:,9)+Y(:,10)+Y(:,11)+Y(:,12)+Y(:,13)+Y(:,14)
+Y(:,15)+Y(:,16)+Y(:,17)+Y(:,19)+Y(:,20),'color','k') %this is total of LR
%
plot(T,Y(:,11)+Y(:,12)+2*Y(:,13)+Y(:,14)+2*Y(:,15)+Y(:,16)+2*Y(:,17)+3*Y(:,
18)+3*Y(:,19)+4*Y(:,20)+4*Y(:,21)+3*Y(:,22)+2*Y(:,23)+3*Y(:,24)+2*Y(:,25)+Y
(:,26)+Y(:,27)+Y(:,28)+2*Y(:,29)+Y(:,30)+Y(:,33),'color','m') %this is
taltal of E
% Y(end,:);
% figure(2),
% plot(T,Y(:,31)),hold on
% plot(T,Y(:,34),'color','k')
% plot(T,Y(:,3),'color','g')
% plot(T,Y(:,5),'color','y')
% plot(T,Y(:,27),'color','r')

%%
BPtotal = sum(Y(:, 1:5), 2)+ sum(Y(:, 21:30), 2);
LRtotal = sum(Y(:, 6:20), 2);
LRfrac= LRtotal./(BPtotal+LRtotal);%final Output

%BPtotalfinal=Y(end,1)+ Y(end,2)+ Y(end,3);
%LRtotalfinal=Y(end,5)+ Y(end,6)+ Y(end,8);
%LRfrac= LRtotalfinal/(BPtotalfinal+LRtotalfinal);%final Output
function dy = DlatchODEs(t,y)
BP=y(1);
BPI=y(2);
BPI2=y(3);
BPI2I=y(4);
BPI2I2=y(5);

LR=y(6);
LRI=y(7);
LRI2=y(8);
LRI2I=y(9);
LRI2I2=y(10);
LRIE=y(11);
LRI2E=y(12);
LRI2E2=y(13);
LRI2IE=y(14);
LRI2IE2=y(15);
LRI2I2E=y(16);
LRI2I2E2=y(17);
LRI2IE2E=y(18);
LRI2I2E2E=y(19);
```

```
LRI2I2E2E2=y(20);

BPI2I2E2E2=y(21);
BPI2I2E2E=y(22);
BPI2I2E2=y(23);
BPI2IE2E=y(24);
BPI2IE2=y(25);
BPI2IE=y(26);
BPI2I2E=y(27);
BPI2E=y(28);
BPI2E2=y(29);
BPIE=y(30);

I=y(31);
I2=y(32);
E=y(33);
int=y(34);
xis=y(35);

 %diffusion limited binding rate 1e8 /M/s = 0.1/nM/s = 6/nM/min
 % to make this simple I would just keep at ~ 1 nM/min (same order of mag)
diffLim = 1; %nM/min
% Dissociation equilbrium constant of integrase dimer (Ki) is unknown; we
just
% gonna use 'a typical' 10 nM Kd as used in Buchler et al 2005 PNAS paper
% table-1. the dissociatio rate, k10 is Ki*diffLim
Ki = 1; % nM
% From Ghosh et al 2005 JMB paper figure-1, dissociation equilibrium
constant for
% integrase dimer - attB or attP site are 70 nM and integrase dimer - attL
% or att R are 15 nM. We just gonna estimate this dissociation equilibrium
% between flippee and integrase dimer (Kdi) at 30 nM. Thus, all the binding
% dissociation rate constant between flipee and integraes dimer (k12, k14,
% k16, k22, )are % approximately diffLim*Kdi
Kdi = 30; % nM
% Intgrase-excisionase dissociation equilibrium constant is unknown. We
% will just use the same number as a `typical' dimerization equilibrium
% constant for protein dimer as we use above (since both cases are
% protein-protein interaction). The dissociation rate constant is thus
% approximately diffLim*Kdix
Kdix = 100; % nM
% Catalytic rate of BP to LR and LR to BP recombinations are unknown. The
% only recombination catalytic rate we have seen are from Ringrose et al
% 1998 JMB paper table-3 which shows the catalytic rate of Cre and Flp to
% be 0.006 /sec and 0.04 /sec, respectively. (~0.36 /min and 2.4 /min,
respectively).
% We will use these as a 'typical' recombination catalytic (kc) rate of
% 1/min.
kc = 10; %/min
% Promoter clearance rate is at the maximal ~ 1 per sec (60 bases per
% second RNAP speed). The number of protein produced per RNA transcript is
% about 10 per mRNA (took this number from Arkin et al 1998 Genetics paper
% table-2). Thus, we can give protein output per gene up to say, 600
molecules
% (nM)per minute. However, in our case, we usually use very weak RBS and
% sometimes gtg start codon and sub optimal promoter. Thus, our protein
output range
% could be much lower.Let's start with 1 nM/gene/min. In our plot we scale
% integrase and excisionase production by scaling 'int' and 'xis' parameter
% value which, in our case, will give the same result as scaling intProd
% and xisProd. In other words, x- and y- axis on the heatmap indicate xis
% and int production in nM/min unit
intProd = 1; %/min
xisProd = 1; %/min
% protein degradation and dilution rate depend on protein stability and
% rate of cell growth, respectively. At the minimal, protein level comes
```

```
% down by cell growth and division. We use a typical E.coli cell cycle of
% 20 min to by a half-life of protein due to dilution so the degradation &
% dilution is at least log(2)/20 /min ~ 0.03/min. With active degradation
% protein half life can go down to a minute (need to check ref, vaguely
% remember from Sauer's lab lambda-ssrA degradation study) to the
% degradation + dilution rate can be as high has log(2)/1 ~ 1 /min. Here we
% just go with an intermediate range of ~ 0.1 min
ky = 1; %/min

dy = zeros(35,1);
k1=0; % BP      + I -> BPI
k2=0; % BP      + I <- BPI
k3=0; % BPI     + I -> BP(I2)
k4=0; % BPI     + I <- BP(I2)
k5=0; % BP(I2)  + I -> BP(I2)I
k6=0; % BP(I2)  + I <- BP(I2)I
k7=0; % BP(I2)I + I -> BP(I4)
k8=0; % BP(I2)I + I <- BP(I4)
k9=diffLim; % I + I       -> I2
k10=Ki*diffLim;% I + I       <- I2

k11=diffLim; % BP     + I2 -> BP(I2)
k12=Kdi*diffLim; % BP     + I2 <- BP(I2)
k13=diffLim; % BP(I2) + I2 -> BP(I4)
k14=Kdi*diffLim; % BP(I2) + I2 <- BP(I4)
k15=kc; % BP(I4)      -> LR(I4)
k16=Kdi*diffLim; % LR(I4)      -> LR(I2)  + I2
k17=diffLim; % LR(I4)      <- LR(I2)  + I2
k18=0; % LR(I4)      -> LR(I2)I + I
k19=0; % LR(I4)      <- LR(I2)I + I
k20=0; %LR(I2)I      -> LR(I2) + I

k21=0; %LR(I2)I <- LR(I2) + I
k22=Kdi*diffLim; %LR(I2)  -> LR + I2
k23=diffLim; %LR(I2)  <- LR + I2
k24=0; %LR(I2)  -> LRI + I
k25=0; %LR(I2)  <- LRI + I
k26=0; %LRI    -> LR + I
k27=0; %LRI    <- LR + I
k28=0;
k29=0;
k30=diffLim; %LR(I2) + E  -> LR(I2)E

k31=Kdix*diffLim; %LR(I2) + E   <- LR(I2)E
k32=diffLim; %LR(I2)E + E  -> LR(I2)(E2)
k33=Kdix*diffLim; %LR(I2)E + E  <- LR(I2)(E2)
k34=0;
k35=0;
k36=0;
k37=0;
k38=0; %LR(I2)I(E2)  + E  -> LR(I2)I(E2)E
k70=0; %LR(I2)I(E2)  + E  <- LR(I2)I(E2)E

k39=diffLim; %LR(I4)       + E  -> LR(I4)E
k40=Kdix*diffLim; %LR(I2)       + E  <- LR(I2)E

k41=diffLim; %LR(I4)E         + E  -> LR(I4)(E2)
k42=Kdix*diffLim; %LR(I4)E         + E  <- LR(I4)(E2)
k43=diffLim; %LR(I4)(E2)      + E  -> LR(I4)(E2)E
k44=Kdix*diffLim; %LR(I4)(E2)      + E  <- LR(I4)(E2)E
k45=diffLim; %LR(I4)(E2)E     + E  -> LR(I4)(E4)
k46=Kdix*diffLim; %LR(I4)(E2)E     + E  <- LR(I4)(E4)
k47=kc; %LR(I4)(E4)        -> BP(I4)(E4)
k48=Kdix*diffLim; %BP(I4)(E4)           -> BP(I4)(E2)E + E
k49=diffLim; %BP(I4)(E4)           <- BP(I4)(E2)E + E
k50=Kdix*diffLim; %BP(I4)(E2)E          -> BP(I4)(E2)  + E
```

```
k51=diffLim; %BP(I4)(E2)E          <- BP(I4)(E2)  + E
k52=Kdix*diffLim; %BP(I4)(E2)           -> BP(I4)E     + E
k53=diffLim; %BP(I4)(E2)           <- BP(I4)E     + E
k54=Kdix*diffLim; % BP(I4)E       -> BP(I4) + E
k55=diffLim; % BP(I4)E       <- BP(I4) + E
k56=0;
k57=0;
k58=0;
k59=0;
k60=0;

k61=0;
k62=Kdix*diffLim; % BP(I2)(E2)       -> BP(I2)E + E
k63=diffLim; % BP(I2)(E2)       <- BP(I2)E + E
k64=Kdix*diffLim; % BP(I2)E          -> BP(I2)  + E
k65=diffLim; % BP(I2)E          <- BP(I2)  + E
k66=0;
k67=0;
k68=intProd; % int -> int + I
k69=xisProd; % xis -> xis + E

k71=ky; % I  -> or I2 -> I
k72=ky; % E  ->


dy(1) = k2*BPI + k12*BPI2 - k1*BP*I - k11*BP*I2; %*** dBP/dt
%%dy(2) = k1*BP*I+k4*BPI2+k66*BPIE-k2*BPI-k3*BPI*I-k67*BPI*E; %*** dBPI/dt

dy(3) = k3*BPI*I - k4*BPI2 - k5*BPI2*I + k6*BPI2I ...
        + k11*BP*I2 - k12*BPI2-k13*BPI2*I2 +k14*BPI2I2 ...
        + k64*BPI2E -k65*BPI2*E;   %*** dBP(I2)/dt

%%dy(4) = k5*BPI2*I+k8*BPI2I2+k60*BPI2IE-k6*BPI2I-k7*BPI2I*I-
k61*BPI2I*E;*** dBP(I2)I/dt

dy(5) = k7*BPI2I*I - k8*BPI2I2 + k13*BPI2*I2 - k14*BPI2I2 ...
        -k15*BPI2I2 ...
        +k54*BPI2I2E - k55*BPI2I2*E; %*** dBP(I4)/dt

dy(6) = +k22*LRI2 - k23*LR*I2 + k26*LRI - k27*LR*I; %*** dLR/dt
%%dy(7) = k24*LRI2+k27*LR*I+k29*LRIE-k25*LRI*I-k26*LRI-k28*LRI*E;
%*** dLRI/dt

dy(8) =   k16*LRI2I2 -k17*LRI2*I2 + k20*LRI2I - k21*LRI2*I ...
         -k22*LRI2 + k23*LR*I2  - k24*LRI2 + k25*LRI*I ...
         -k30*LRI2*E + k31*LRI2E; % dLR(I2)/dt

%%dy(9) = k18*LRI2I2+k21*LRI2*I+k35*LRI2IE-k19*LRI2I*I-k20*LRI2I-
k34*LRI2I*E;
%*** dLR(I2)I/dt

dy(10) = k15*BPI2I2 ...
         - k16*LRI2I2 + k17*LRI2*I2 - k18*LRI2I2 + k19*LRI2I*I ...
         - k39*LRI2I2*E + k40*LRI2I2E; %*** dLR(I4)/dt
%%dy(11) = k28*LR*E-k29*LRIE; %*** dLRIE/dt

dy(12) = k30*LRI2*E -k31*LRI2E -k32*LRI2E*E + k33*LRI2E2; % dLR(I2)E/dt

dy(13) = k32*LRI2E*E - k33*LRI2E2;% dLR(I2)(E2)/dt

%%dy(14) = k34*LRI2I*E+k37*LRI2I2E2-k35*LRI2IE-k36*LRI2IE*E; dLR(I2)IE/dt

dy(15) = k36*LRI2IE*E - k37*LRI2IE2 -k38*LRI2IE2*E + k70*LRI2IE2E;%
```

```
dLR(I2)I(E2)/dt

dy(16) = k39*LRI2I2*E - k40*LRI2I2E - k41*LRI2I2E*E + k42*LRI2I2E2 ;%
dLR(I4)E/dt

dy(17) = k41*LRI2I2E*E - k42*LRI2I2E2 - k43*LRI2I2E2*E + k44*LRI2I2E2E;%
dLR(I4)(E2)/dt

%%dy(18) = k38*LRI2IE2*E-k70*LRI2IE2E; % dLR(I2)I(E2)/dt

dy(19) =    k43*LRI2I2E2*E  - k44*LRI2I2E2E ...
         - k45*LRI2I2E2E*E + k46*LRI2I2E2E2; % dLR(I4)(E2)E/dt

dy(20) = k45*LRI2I2E2E*E-k46*LRI2I2E2E2 ...
        -k47*LRI2I2E2E2; % dLR(I4)(E4)/dt

dy(21) =   k47*LRI2I2E2E2 ...
         - k48*BPI2I2E2E2 + k49*BPI2I2E2E*E ; % dBP(I4)(E4)/dt

dy(22) =  k48*BPI2I2E2E2 - k49*BPI2I2E2E*E ...
         -k50*BPI2I2E2E  +  k51*BPI2I2E2*E; % dBP(I4)(E2)E/dt

dy(23) =  k50*BPI2I2E2E -k51*BPI2I2E2*E ...
         -k52*BPI2I2E2 + k53*BPI2I2E*E; % dBP(I4)(E2)/dt

%%dy(24) = k57*BPI2IE2*E-k56*BPI2IE2E; % dBP(I2)I(E2)E/dt
%%dy(25) = k56*BPI2IE2E+k59*BPI2IE*E-k57*BPI2IE2*E-k58*BPI2IE2;
%%%dBP(I2)I(E2)/dt

%%dy(26) = k58*BPI2IE2+k61*BPI2I*E-k59*BPI2IE*E-k60*BPI2IE;
%%%dBP(I2)IE/dt

dy(27) = k52*BPI2I2E2 -k53*BPI2I2E*E - k54*BPI2I2E + k55*BPI2I2*E; %
dBP(I4)E/dt

dy(28) = k62*BPI2E2 - k63*BPI2E*E - k64*BPI2E + k65*BPI2*E;% dBP(I2)E/dt

dy(29) = -k62*BPI2E2 + k63*BPI2E*E; % dBP(I2)(E2)/dt

%%dy(30) = k67*BPI*E-k66*BPIE; % dBPIE/dt

dy(31) = -k1*BP*I   + k2*BPI    -k3*BPI*I   + k4*BPI2 ...
         -k5*BPI2*I + k6*BPI2I  -k7*BPI2I*I + k8*BPI2I2 ...
         -k9*I*I    + 2*k10*I2  +k18*LRI2I2 - k19*LRI2I*I ...
         +k20*LRI2I -k21*LRI2*I +k24*LRI2   - k25*LRI*I ...
         +k26*LRI-k27*LR*I ...
         +k68*int ...
         -k71*I ...
         +k71*I2; %% this one for dimer degrades to monomer
         % dI/dt

dy(32) = +0.5*k9*I*I  - k10*I2     - k11*BP*I2  + k12*BPI2 ...
         -k13*BPI2*I2 + k14*BPI2I2 + k16*LRI2I2 - k17*LRI2*I2 ...
         +k22*LRI2 - k23*LR*I2 ...
         -k71*I2;  %% this one for dimer degrades to monomer
         % d(I2)/dt

dy(33) =  -k28*LRI*E       + k29*LRIE ...
          -k30*LRI2*E      + k31*LRI2E ...
          -k32*LRI2E*E     + k33*LRI2E2 ...
          -k34*LRI2I*E     + k35*LRI2IE ...
          -k36*LRI2IE*E    + k37*LRI2IE2 ...
          -k38*LRI2IE2*E   + k70*LRI2IE2E ...
```

```
          -k39*LRI2I2*E    + k40*LRI2I2E ...
          -k41*LRI2I2E*E   + k42*LRI2I2E2 ...
          -k43*LRI2I2E2*E  + k44*LRI2I2E2E ...
          -k45*LRI2I2E2E*E + k46*LRI2I2E2E2 ...
          +k48*BPI2I2E2E2  - k49*BPI2I2E2E*E ...
          +k50*BPI2I2E2E   - k51*BPI2I2E2*E ...
          +k52*BPI2I2E2    - k53*BPI2I2E*E ...
          +k54*BPI2I2E     - k55*BPI2I2*E ...
          +k56*BPI2IE2E    - k57*BPI2IE2*E ...
          +k58*BPI2IE2     - k59*BPI2IE*E ...
          +k60*BPI2IE      - k61*BPI2I*E ...
          +k62*BPI2E2      - k63*BPI2E*E ...
          +k64*BPI2E       - k65*BPI2*E ...
          +k66*BPIE        - k67*BPI*E ...
          +k69*xis ...
          -k72*E; % d(I2)/dt
 LRI2I*E;
%*** dLR(I2)I/dt

dy(10) = k15*BPI2I2 ...
         - k16*LRI2I2 + k17*LRI2*I2 - k18*LRI2I2 + k19*LRI2I*I ...
         - k39*LRI2I2*E + k40*LRI2I2E; %*** dLR(I4)/dt
%%dy(11) = k28*LR*E-k29*LRIE; %*** dLRIE/dt

dy(12) = k30*LRI2*E -k31*LRI2E -k32*LRI2E*E + k33*LRI2E2; % dLR(I2)E/dt

dy(13) = k32*LRI2E*E - k33*LRI2E2;% dLR(I2)(E2)/dt

%%dy(14) = k34*LRI2I*E+k37*LRI2I2E2-k35*LRI2IE-k36*LRI2IE*E; dLR(I2)IE/dt

dy(15) = k36*LRI2IE*E - k37*LRI2IE2 -k38*LRI2IE2*E + k70*LRI2IE2E;%
dLR(I2)I(E2)/dt

dy(16) = k39*LRI2I2*E - k40*LRI2I2E - k41*LRI2I2E*E + k42*LRI2I2E2 ;%
dLR(I4)E/dt

dy(17) = k41*LRI2I2E*E - k42*LRI2I2E2 - k43*LRI2I2E2*E + k44*LRI2I2E2E;%
dLR(I4)(E2)/dt

%%dy(18) = k38*LRI2IE2*E-k70*LRI2IE2E; % dLR(I2)I(E2)/dt

dy(19) =    k43*LRI2I2E2*E  - k44*LRI2I2E2E ...
          - k45*LRI2I2E2E*E + k46*LRI2I2E2E2; % dLR(I4)(E2)E/dt

dy(20) = k45*LRI2I2E2E*E-k46*LRI2I2E2E2 ...
        -k47*LRI2I2E2E2; % dLR(I4)(E4)/dt

dy(21) =   k47*LRI2I2E2E2 ...
         - k48*BPI2I2E2E2 + k49*BPI2I2E2E*E ; % dBP(I4)(E4)/dt

dy(22) =  k48*BPI2I2E2E2 - k49*BPI2I2E2E*E ...
         -k50*BPI2I2E2E  +  k51*BPI2I2E2*E; % dBP(I4)(E2)E/dt

dy(23) =  k50*BPI2I2E2E -k51*BPI2I2E2*E ...
         -k52*BPI2I2E2 + k53*BPI2I2E*E; % dBP(I4)(E2)/dt

%%dy(24) = k57*BPI2IE2*E-k56*BPI2IE2E; % dBP(I2)I(E2)E/dt
%%dy(25) = k56*BPI2IE2E+k59*BPI2IE*E-k57*BPI2IE2*E-k58*BPI2IE2;
%%%dBP(I2)I(E2)/dt

%%dy(26) = k58*BPI2IE2+k61*BPI2I*E-k59*BPI2IE*E-k60*BPI2IE;
%%%dBP(I2)IE/dt

dy(27) = k52*BPI2I2E2 -k53*BPI2I2E*E - k54*BPI2I2E + k55*BPI2I2*E; %
```

```
dBP(I4)E/dt

dy(28) = k62*BPI2E2 - k63*BPI2E*E - k64*BPI2E + k65*BPI2*E;% dBP(I2)E/dt

dy(29) = -k62*BPI2E2 + k63*BPI2E*E; % dBP(I2)(E2)/dt

%%dy(30) = k67*BPI*E-k66*BPIE; % dBPIE/dt

dy(31) = -k1*BP*I   + k2*BPI    -k3*BPI*I   + k4*BPI2 ...
         -k5*BPI2*I + k6*BPI2I  -k7*BPI2I*I + k8*BPI2I2 ...
         -k9*I*I    + 2*k10*I2  +k18*LRI2I2 - k19*LRI2I*I ...
         +k20*LRI2I -k21*LRI2*I +k24*LRI2   - k25*LRI*I ...
         +k26*LRI-k27*LR*I ...
         +k68*int ...
         -k71*I ...
         +k71*I2; %% this one for dimer degrades to monomer
         % dI/dt

dy(32) = +0.5*k9*I*I  - k10*I2     - k11*BP*I2  + k12*BPI2 ...
         -k13*BPI2*I2 + k14*BPI2I2 + k16*LRI2I2 - k17*LRI2*I2 ...
         +k22*LRI2 - k23*LR*I2 ...
         -k71*I2;  %% this one for dimer degrades to monomer
         % d(I2)/dt

dy(33) =  -k28*LRI*E       + k29*LRIE ...
          -k30*LRI2*E      + k31*LRI2E ...
          -k32*LRI2E*E     + k33*LRI2E2 ...
          -k34*LRI2I*E     + k35*LRI2IE ...
          -k36*LRI2IE*E    + k37*LRI2IE2 ...
          -k38*LRI2IE2*E   + k70*LRI2IE2E ...
          -k39*LRI2I2*E    + k40*LRI2I2E ...
          -k41*LRI2I2E*E   + k42*LRI2I2E2 ...
          -k43*LRI2I2E2*E  + k44*LRI2I2E2E ...
          -k45*LRI2I2E2E*E + k46*LRI2I2E2E2 ...
          +k48*BPI2I2E2E2  - k49*BPI2I2E2E*E ...
          +k50*BPI2I2E2E   - k51*BPI2I2E2*E ...
          +k52*BPI2I2E2    - k53*BPI2I2E*E ...
          +k54*BPI2I2E     - k55*BPI2I2*E ...
          +k56*BPI2IE2E    - k57*BPI2IE2*E ...
          +k58*BPI2IE2     - k59*BPI2IE*E ...
          +k60*BPI2IE      - k61*BPI2I*E ...
          +k62*BPI2E2      - k63*BPI2E*E ...
          +k64*BPI2E       - k65*BPI2*E ...
          +k66*BPIE        - k67*BPI*E ...
          +k69*xis ...
          -k72*E; % d(I2)/dt
```

Schematic workflow for measurement vector project:

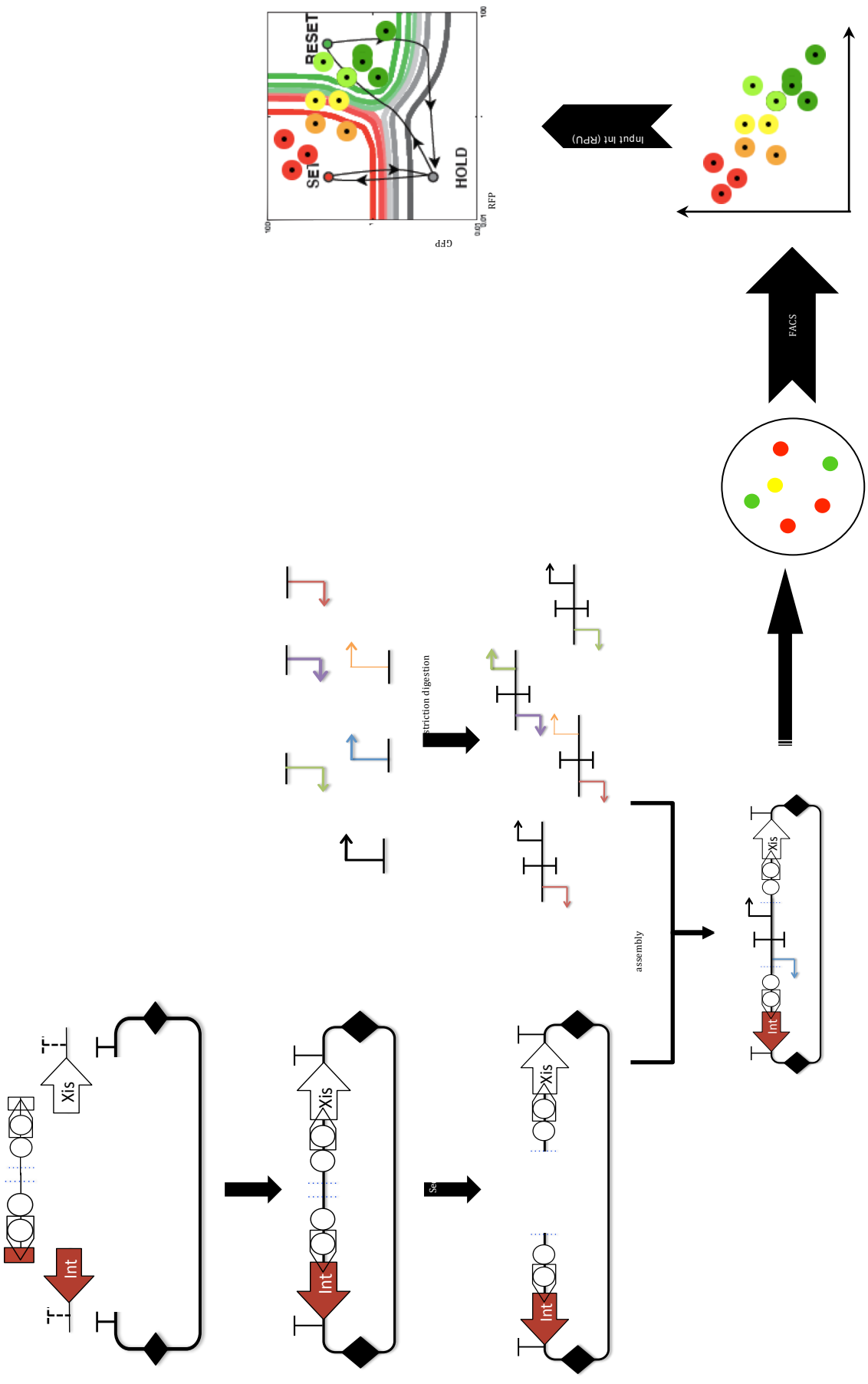

Erklärung

Hiermit versichere ich, Nicolas Koutsoubelis, dass ich die vorliegende Arbeit selbstständig verfasst habe, keine anderen als die angegebenen Quellen und Hilfsmittel benutzt habe, alle verwendeten Bilder und Graphiken mit der Genehmigung des Autors verwendet wurden und dass die Arbeit bisher oder gleichzeitig keiner anderen Prüfungsbehörde unter Erlangung eines akademischen Grades vorgelegt wurde.

Ort, Datum Unterschrift